identified. Peroxisomes were easily detected because of their high contrast because of the positive DAB reaction. In each frame, the number of peroxisomal profiles and the area of each individual profile were determined. The numerical density and volume density of peroxisomes were calculated using the following equations: numerical density (number/μm^2) = $N_P/(A_T - A_{empty})$, and volume density (%) = $A_{TP}/(A_T - A_{empty}) \times 100$, where N_P is the peroxisome number in the test area, A_T is the test area, A_{empty} is the area of the vascular and biliary lumens and that of the hepatocyte nuclei and lipid droplets, and A_{TP} is the area of total peroxisomal profiles in the test area. The area was measured with a Luzex AP image analyzer (Nireco, Tokyo, Japan).

Immunofluorescence staining

Liver samples were fixed in 4% paraformaldehyde in phosphate-buffered saline (PBS), embedded in Tissue-Tek O.C.T compound™ (Sakura Finetek, Torrance, CA) and frozen. Frozen liver 5-μm sections were prepared, washed with PBS, blocked with bovine serum albumin for 1 hr and incubated overnight with rabbit polyclonal antibodies against cyclin D1 (1:50 dilution)[19] and PPARα (1:100 dilution),[18] and with mouse monoclonal antibody against proliferating cell nuclear antigen (PCNA) (1:100 dilution).[19] After 5 washes with PBS, these sections were incubated with fluorescein isothiocyanate (FITC)-conjugated goat anti-rabbit IgG (Jackson ImmunoResearch, West Grove, PA) or donkey anti-mouse IgG (Dako). The sections were mounted and viewed with an Olympus Fluoview confocal laser scanning microscope (Olympus, Tokyo, Japan). Two-thousand hepatocyte nuclei were examined for each mouse, and the number of hepatocyte nuclei stained with the antibodies against cyclin D1, PPARα and PCNA was counted and expressed as a percentage.

Assessment of apoptotic hepatocytes

Liver samples were cut into small pieces and then fixed in 4% paraformaldehyde in PBS. These samples were dehydrated, embedded in paraffin and cut into 4-μm sections. The terminal deoxynucleotidyl transferase-mediated deoxyuridine triphosphate nick-end labeling (TUNEL) assay was performed using a MEBSTAIN Apoptosis Kit II (Medical and Biological Laboratories, Nagoya, Japan). The number of apoptotic hepatocytes in 2,000 hepatocytes was counted for each mouse, and expressed as a percentage.

Other methods

Hepatic caspase 3 activity was measured as described elsewhere.[23] For analysis of the nuclear contents of nonesterified fatty acids (NEFAs), ~150 μL of the hepatocyte nuclear fraction, containing 1–2 mg of protein, was treated with a microsonicator. Lipid extraction was performed according to a modification of the method developed by Folch *et al.*[24] and the nuclear content of NEFAs was measured with a *NEFA* C-test kit™ (Wako).

Statistical analysis

Statistical analysis was performed by means of Student's *t*-test. The results are expressed as the mean ± standard deviation. A probability value of less than 0.05 was considered to be statistically significant.

Results

Accelerated hepatocyte proliferation in HCV core gene transgenic mice

To evaluate hepatocyte proliferative activity, PCNA-positive hepatocytes were counted in male transgenic mice and nontransgenic mice. Although hepatic inflammation and hepatocyte necrosis were not detected in either group, the numbers of PCNA-positive hepatocytes were significantly increased in the 9-month-old transgenic mice compared with the 9-month-old nontransgenic mice (Fig. 1*a*). The increase was more significant in the 22-month-old transgenic mice (Fig. 1*a*). The numbers of PCNA-positive hepatocytes in the 22-month-old transgenic mice corresponded with those in HCV polyprotein-expressing transgenic mice with HCC.[25] On the other hand, the parameters of apoptosis, *i.e.*, the numbers of TUNEL-positive hepatocytes and hepatic caspase 3 activity, remained unchanged between the 2 groups at the same ages (Figs. 1*b* and 1*c*). These results suggest that spontaneous hepatocyte proliferation occurs as early as the age of 9 months and persists for a long time in HCV core gene transgenic mice.

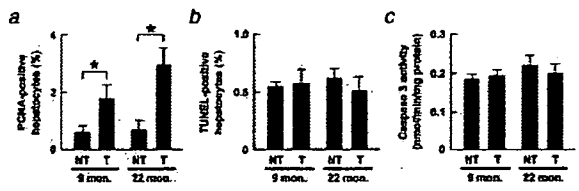

FIGURE 1 – Increase in hepatocyte proliferative activity. (*a*) The number of PCNA-positive hepatocytes. Two-thousand hepatocyte nuclei were examined for each mouse, and the number stained with anti-PCNA antibody was counted. Results are expressed as the mean ± standard deviation (n = 8). *, $p < 0.05$ between the transgenic mice and the nontransgenic mice; NT, nontransgenic mice; T, transgenic mice; 9 mon, 9-month-old mice; 22 mon, 22-month-old mice. (*b*) The number of apoptotic hepatocytes. The number of TUNEL-positive hepatocytes in 2,000 hepatocytes was determined for each mouse. Results are expressed as the mean ± standard deviation (n = 8). (*c*) Caspase 3 activity. Results are expressed as the mean ± standard deviation (n = 8).

Simultaneous induction of cell-cycle regulators and oncogene products in HCV core gene transgenic mouse livers

To examine the changes in the expression of proteins associated with hepatocyte division, the livers of the 9- and 22-month-old mice were subjected to immunoblot analysis. The levels of many proteins including cell-cycle regulators [cyclin-dependent kinase (CDK) 1, 2 and 4, cyclin D1 and E, and PCNA], and oncogene products (c-Myc, c-Fos and c-Ha-Ras) were significantly higher in the 22-month-old transgenic mice than in the control mice (Fig. 2). The levels of CDK inhibitors such as p16 and p21 were similar between the 2 groups. Similar results were obtained from the 9-month-old transgenic mice (data not shown). Time course changes in the expression of key G1-S checkpoint regulators, cyclin D1 and CDK4, are shown in Figure 3*a*. The simultaneous increase in the expression of cyclin D1 and CDK4 in the transgenic mice was continuous and more pronounced with age. Northern blot analysis revealed that the increase of these proteins occurred at the transcriptional level (Figs. 3*b* and 3*c*). Thus, these results reveal that various proteins which accelerate cell-cycle progression were induced simultaneously, persistently and age-dependently in the transgenic mice.

Correlative induction of PPARα targets in HCV core gene transgenic mouse livers

As shown in Figure 2, the expression of many kinds of cell-cycle regulators and oncogene products is known to be induced by the functional activation of PPARα.[19,26–30] To investigate whether PPARα is activated in the livers of transgenic mice, the expression of representative PPARα target genes,[30] acyl-CoA oxidase (AOX), peroxisomal thiolase (PT) and liver-type fatty acid-binding protein (L-FABP), was examined. As demonstrated in Figure 3*a*, the levels of AOX, PT, and L-FABP were increased in the 9-month-old transgenic mice compared with the nontransgenic mice, and the increase was more pronounced in the 22-month-old transgenic mice. Northern blot analysis demonstrated that the increase in these PPARα targets was based on the increase in the transcriptional activity (Figs. 3*b* and 3*c*). The increase in the

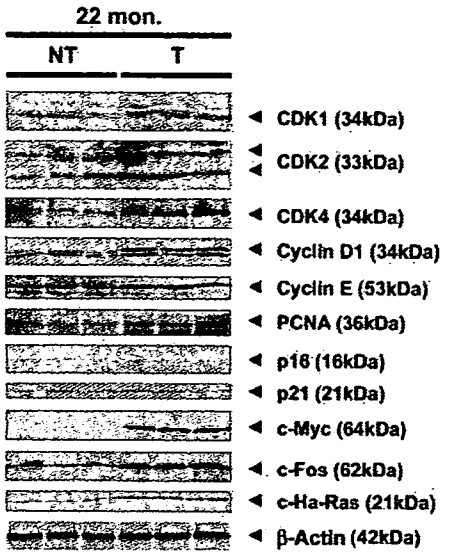

FIGURE 2 – Immunoblot analysis of cell-cycle regulators and oncogene products. Whole liver lysate (200 μg) was loaded in each lane. The band of β-actin was used as the loading control. The apparent molecular weight is indicated in parentheses. 22 mon, 22-month-old mice; NT, nontransgenic mice; T, transgenic mice.

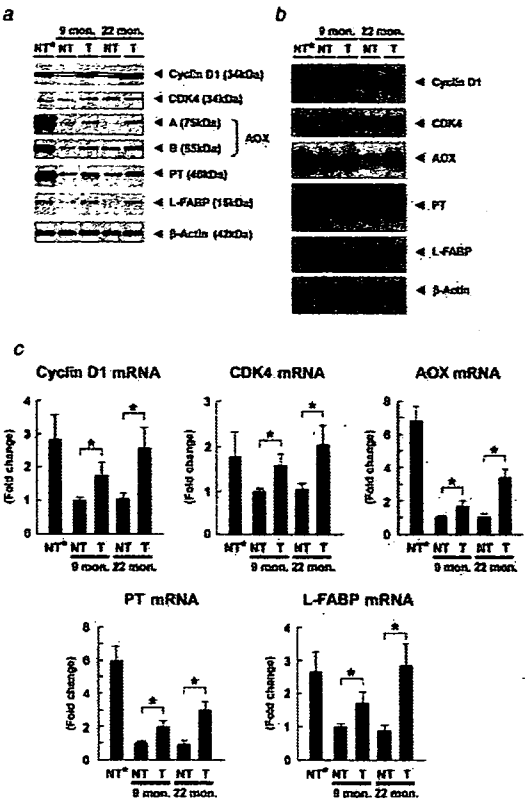

FIGURE 3 – Analysis of PPARα-regulated proteins. (*a*) Immunoblot analysis of cell-cycle regulators and fatty acid-metabolizing enzymes and proteins. Since no significant individual differences in the same mouse group were found in the preliminary experiments, 10 mg of liver pieces prepared from each mouse (n = 8/group) was mixed and homogenized. Whole liver lysate (200 μg for cyclin D1 and CDK4, and 20 μg for others) was loaded in each lane. The band of β-actin was used as the loading control. Results are representative of 4 independent experiments. The apparent molecular weight is indicated in parentheses. 9 mon, 9-month-old mice; 22 mon, 22-month-old mice; NT, nontransgenic mice; T, transgenic mice; NT*, nontransgenic mice treated with a control diet containing 0.5% clofibrate for 2 weeks; A and B, full-length and truncated AOX, respectively. (*b*) Northern blot analysis concerning the proteins in (*a*). Ten milligram of liver pieces from each mouse (n = 8/group) was mixed and homogenized, and total liver RNA was extracted. Hepatic RNA (5 μg) was separated on a denaturing gel, transferred to membranes and hybridized with the indicated ^{32}P-labeled cDNA probes. The blot of β-actin was used as the internal control. Results are representative of 4 independent experiments. (*c*) Quantification of hepatic mRNA levels. The mRNA level was quantified using a phosphorimager, normalized to that of β-actin, and subsequently normalized to that of 9-month-old nontransgenic mice. Results were obtained from 4 independent experiments and expressed as the mean ± standard deviation. Abbreviations are identical with those in (*b*). *, $p < 0.05$ between the transgenic mice and the nontransgenic mice.

mRNA expression of AOX, PT and L-FABP corresponded exactly with that of cyclin D1 or CDK4 (Figs. 3*b* and 3*c*). Therefore, these results demonstrate the strong correlation between continuous and age-dependent induction of cell-cycle regulators and functional activation of PPARα in these transgenic mice. Furthermore, the induction of these 5 proteins was also observed in wild-type mice treated with clofibrate, a potent PPARα activator; however, the degree of the induction of AOX and PT in the transgenic mice was smaller than that in the clofibrate-treated wild-type mice (Fig. 3), suggesting that the PPARα activation found in the transgenic mice was not as intense as that in the mice treated with clofibrate.

Histological evaluation of PPARα activation

An increase in the numbers of peroxisomes is associated with PPARα activation.[18] To determine whether peroxisome proliferation occurs in the HCV core gene transgenic mice, cytochemical staining for peroxisomal catalase was performed. A scattered distribution of hepatocytes with numerous peroxisomes was observed in the 9-month-old transgenic mice (Fig. 4*a*). Such hepatocytes were also found in the 22-month-old transgenic mouse livers (Fig. 4*a*). In contrast, almost all of the hepatocytes in the clofibrate-treated mice showed significant peroxisome proliferation (Fig. 4*a*). To quantitatively evaluate the degree of peroxisome proliferation, morphometric analysis of peroxisomes was conducted. The numerical density and volume density were significantly increased in the transgenic mice compared with those in the nontransgenic mice (Fig. 4*b*). The volume density, the most reliable parameter of peroxisome proliferation, was increased age-dependently in the transgenic mice, but the degree of the increase was not as prominent as that observed in mice with clofibrate administration (Fig. 4*b*). The finding that only some hepatocytes in the transgenic mice presented a marked peroxisome proliferation (Fig. 4*a*) is noteworthy, since it seems to correlate with the finding that intense expression of the core protein was observed only in particular hepatocytes.[10] These histological analyses reveal that spontaneous, continuous and age-dependent peroxisome proliferation and PPARα activation occur heterogeneously in the transgenic mouse livers, which is different from the response observed in the mice receiving clofibrate treatment.

Appearance of PPARα-, and cyclin D1-positive hepatocytes

We tried to detect abnormal hepatocytes to clarify the mechanism of hepatocarcinogenesis in the transgenic mice. On PPARα immunofluorescence staining, PPARα was primarily detected in the cytoplasm of the nontransgenic mice and the clofibrate-administered mice. Some hepatocytes having nuclei positively stained

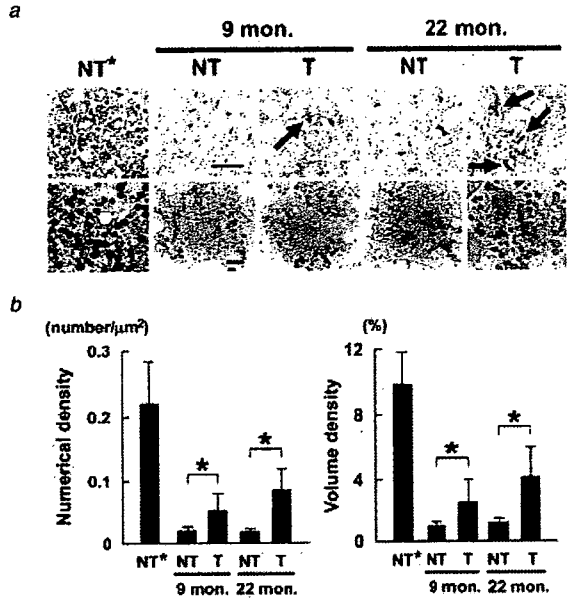

FIGURE 4 – Cytochemical staining for hepatic peroxisomes. (*a*) Light and electron photomicrographs of DAB-stained liver tissues. Peroxisomes are detected as darkly stained particles. The arrows in upper panels indicate hepatocytes showing profound peroxisome proliferation. The bars in the light and electron photomicrographs of 9-month-old nontransgenic mice indicate 50 and 2 μm, respectively. 9 mon, 9-month-old mice; 22 mon, 22-month-old mice; NT, nontransgenic mice; T, transgenic mice; NT*, nontransgenic mice treated with a control diet containing 0.5% clofibrate for 2 weeks. (*b*) Morphometric analysis of hepatic peroxisomes. The number of peroxisomes and the area of each individual peroxisome profile were measured in 10 photomicrographs for each mouse, and morphometric parameters such as numerical density and volume density were calculated. Results are expressed as the mean ± standard deviation ($n = 8$). Abbreviations are identical with those in (*a*). *, $p < 0.05$ between the transgenic mice and the nontransgenic mice.

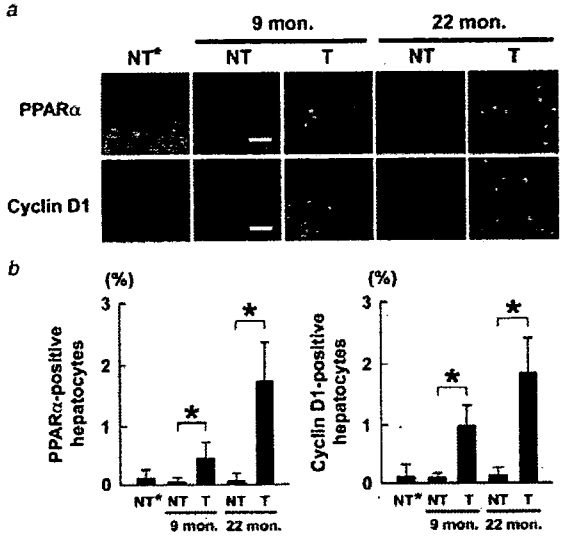

FIGURE 5 – Immunofluorescence staining for PPARα and cyclin D1. (*a*) Immunofluorescence staining using antibodies against PPARα and cyclin D1. The bars in the photomicrographs of 9-month-old nontransgenic mice indicate 50 μm. 9 mon, 9-month-old mice; 22 mon, 22-month-old mice; NT, nontransgenic mice; T, transgenic mice; NT*, nontransgenic mice treated with a control diet containing 0.5% clofibrate for 2 weeks. (*b*) The number of PPARα-, or cyclin D1-positive hepatocytes. Two-thousand hepatocyte nuclei were examined for each mouse, and the number of nuclei intensively stained with anti-PPARα or anti-cyclin D1 antibody was counted. Results are expressed as the mean ± standard deviation ($n = 8$). Abbreviations are identical with those of (*a*). *, $p < 0.05$ between the transgenic mice and the nontransgenic mice.

by anti-PPARα antibody were detected only in the transgenic mice (Fig. 5*a*). Similar to the case of PPARα, the hepatocytes having nuclei stained intensively by anti-cyclin D1 antibody were found only in the transgenic mice (Fig. 5*a*). A few hepatocytes stained by anti-CDK4 antibody were also observed only in the transgenic mice (data not shown). The frequency of appearance of PPARα-, or cyclin D1-positive hepatocytes was increased with age (Figs. 5*a* and 5*b*). Thus, the appearance of these specific hepatocytes in the transgenic mice seemed to be, at least in part, associated with sustained, age-dependent and heterogeneous PPARα activation in the transgenic mice.

Changes in PPARα levels

Since the expression of PPARα is known to be enhanced by its activation,[18,30] the quantitative change in PPARα was evaluated. The nuclear PPARα level in the transgenic mice was increased age-dependently, as expected (Figs. 6*a*, upper panel and 6*b*), but the PPARα level in the whole liver lysate remained unchanged (data not shown). The increase in nuclear PPARα in the transgenic mice was smaller than that in the clofibrate-treated wild-type mice (Figs. 6*a*, upper panel and 6*b*). Northern blot analysis revealed a higher PPARα mRNA level in the clofibrate-treated mice than in the controls, although this parameter in the transgenic mouse groups of each age was similar to that in the controls (Figs. 6*a*, lower panel and 6*b*). These results indicate that the increase in nuclear PPARα in the transgenic mice occurs mainly at the post-transcriptional level, which is distinct from that observed in the clofibrate-treated wild-type mice.

Stabilization of PPARα through a possible interaction with HCV core protein in hepatocyte nuclei

The increased stability of PPARα in hepatocyte nuclei is thought to be one of the possible causes of a disproportional increase in the nuclear PPARα level. To examine this possibility, a pulse-chase experiment was performed using isolated hepatocytes. The half-life of nuclear PPARα was ~7 hr in the control mice and 12.5 hr in the transgenic mice (Fig. 7*a*). In addition, the intensity of the labeled PPARα band (P in Fig. 7*a*, upper panels) in the control mice was similar to that in the transgenic mice. The finding that the [^{35}S]methionine uptake in the hepatocytes from the control mice was similar to that from the transgenic mice suggests that the increase in nuclear PPARα in the hepatocytes from the transgenic mice (Fig. 7*a*, lower right panel), as well as that *in vivo* (Fig. 6*a*, upper panel), is not because of the increased PPARα transfer into the nucleus.

In the transgenic mice, HCV core protein accumulated in the nuclei, as evidenced by immunoelectron microscopy,[11] suggesting a possible interaction of the core protein with PPARα in the nuclei. We therefore examined this possibility by anti-PPARα IgG affinity chromatography. When proteins combining with PPARα in hepatocyte nuclei were subjected to immunoblot analysis, the core protein was clearly detected (Fig. 7*b*). This result suggests the possibility of complex formation between the HCV core protein and PPARα, which is consistent with an interaction of the core protein with retinoid X receptor (RXR) α,[31] an essential heterodimeric partner of PPARα.[32] Thus, HCV core protein may

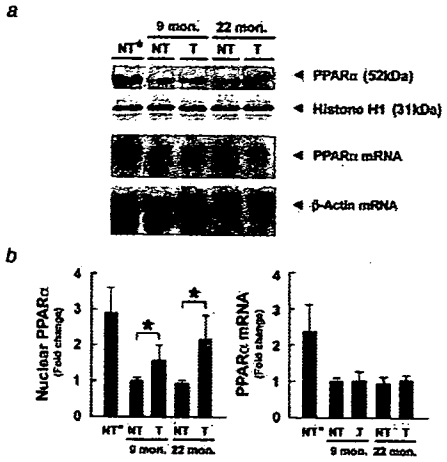

FIGURE 6 – Analysis of PPARα. (*a*) (Upper panels) Immunoblot analysis of nuclear PPARα. Since few individual differences in the same mouse group were found in the preliminary experiments, 30 mg of liver pieces from each mouse (n = 8/group) was mixed and homogenized to prepare the nuclear fraction. One-hundred microgram of nuclear protein was separated on 10% SDS-polyacrylamide gel, transferred to nitrocellulose membranes and reacted with antibody against PPARα. The band of histone H1 was used as the loading control. Results are representative of 4 independent experiments. The apparent molecular weight is indicated in parentheses: 9 mon, 9-month-old mice; 22 mon, 22-month-old mice; NT, nontransgenic mice; T, transgenic mice; NT*, nontransgenic mice treated with a control diet containing 0.5% clofibrate for 2 weeks. (Lower panels) Northern blot analysis of PPARα. A sample used in Figure 3*b* was adopted. Hepatic RNA (5 μg) was electrophoresed and hybridized with cDNAs for PPARα and β-actin, respectively. Results are representative of 4 independent experiments. (*b*) Quantification of nuclear PPARα levels and PPARα mRNA levels. The nuclear PPARα level was quantified densitometrically and normalized to the histone H1 level. The mRNA level of PPARα was quantified using a phosphorimager and normalized to that of β-actin. Values were subsequently normalized to those of 9-month-old nontransgenic mice. Results were obtained from 4 independent experiments and expressed as the mean ± standard deviation. Abbreviations are identical with those in (*a*). *, $p < 0.05$ between the transgenic mice and the nontransgenic mice.

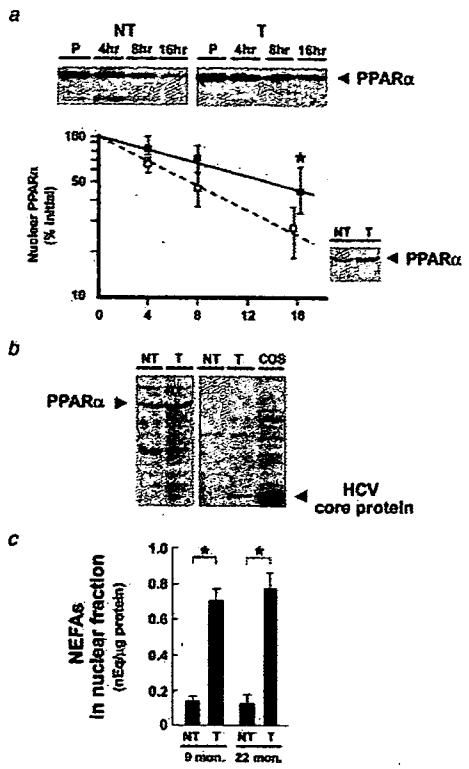

FIGURE 7 – Analyses of PPARα stability, interaction between PPARα with the core protein in hepatocyte nuclei, and nuclear contents of NEFAs. (*a*) Pulse-label and pulse-chase experiments for nuclear PPARα using isolated mouse hepatocytes. (Upper panels) Labeled PPARα bands on X-ray film. Pulse-label and pulse-chase experiments were performed as described in the Material and methods. NT, nontransgenic mice; T, transgenic mice; P, pulse-label; 4, 8, 16 hr, pulse-chase for 4, 8, 16 hr, respectively. (Lower left panel) Intensity plot of PPARα in 5 independent experiments. Values are normalized as a percentage of the values of the pulse-labeled band and expressed as the mean ± standard deviation. Open square, nontransgenic mice; black square, transgenic mice; *, $p < 0.05$ between the transgenic mice and the nontransgenic mice. (Lower right panel) Immunoblot analysis of an isolated hepatocyte nuclear fraction. NT, nontransgenic mice; T, transgenic mice. (*b*) Interaction between PPARα and HCV core protein in the nucleus. (Left panel) Immunoblot analysis (PPARα) of the eluate on anti-PPARα IgG affinity column chromatography. (Right panel) Immunoblot analysis (HCV core protein) of the same eluate. NT, nontransgenic mice; T, transgenic mice; COS, HCV core protein-overexpressing COS cell lysate. (*c*) Nuclear contents of NEFAs. The levels of NEFAs were measured using a hepatocyte nuclear fraction. Results are expressed as the mean ± standard deviation (n = 8). *, $p < 0.05$ between the transgenic mice and the nontransgenic mice; NT, nontransgenic mice; T, transgenic mice; 9 mon, 9-month-old mice; 22 mon, 22-month-old mice.

directly or indirectly affect the stability of PPARα in hepatocyte nuclei.

Increase in PPARα ligands

PPARα is a ligand-activated transcription factor. Since the transgenic mice were fed a standard laboratory chow, endogenous substances such as NEFAs would serve as ligands of PPARα[33]; therefore, the contents of NEFAs in hepatocyte nuclei were compared between the 2 groups. The levels of NEFAs in hepatocyte nuclei in the transgenic mice were ~5 times higher than those in the control mice at the same age (Fig. 7*c*). This could account for the higher activation of PPARα in the transgenic mice than in the controls.

Discussion

A large number of variables are involved in the induction of HCC by HCV core protein. While the precise mechanism underlying hepatocarcinogenesis in HCV core gene transgenic mice cannot be fully elucidated from this study, our results could provide some clues to explain this phenomenon. We found spontaneous, persistent, age-dependent and heterogeneous PPARα activation in the transgenic mouse livers for the first time. This study thus advances our understanding of the association between HCV core protein-mediated hepatocarcinogenesis and persistent PPARα activation.

Hepatocyte proliferation is influenced by various factors, such as mitogenic chemicals, cytokines, growth factors and transcription factors. It has been reported that various kinds of cell-cycle regulators and oncogene products are induced by PPARα activation.[19,26–30] In particular, cyclin D1, CDK4, PCNA and c-Myc are potent and critical regulators of the G1-S checkpoint and cell-cycle progression,[13,14] and aberrant expression of these proteins is frequently detected in HCV-related HCC.[34–37] These key regulators are known to be induced in a PPARα-dependent manner in mice[19,30]; the continuous induction of these proteins and the

resultant acceleration of hepatocyte proliferation found in the transgenic mice may be attributed to persistent PPARα activation. In the current study, we demonstrated that there was a great variety of the intensity of PPARα activation among different hepatocytes (Fig. 4). This persistent and heterogeneous PPARα activation found especially in the transgenic mice may be linked with the age-dependent and multicentric hepatocarcinogenesis induced by the core protein.

It is well-known that the long-term administration of potent peroxisome proliferators such as fibrate drugs can induce hepatocarcinogenesis in rodents.[29] The findings observed in the transgenic mice markedly differ from those in mice with long-term treatment of peroxisome proliferators in several ways. Namely, the transgenic mice show no intense increase in AOX and PT (Fig. 3), no increase in PPARα mRNA (Fig. 6), heterogeneous peroxisome proliferation (Fig. 4) and age-dependent emergence of hepatocytes having nuclei stained intensively by anti-PPARα or anti-cyclin D1 antibody (Fig. 5). Therefore, the mode of PPARα activation and the mechanism of hepatocarcinogenesis caused by HCV core protein expression are indeed unique.

One of the mechanisms involved in the core protein-specific PPARα activation in mice is stabilization of PPARα in hepatocyte nuclei through a possible interaction with the core protein. In cultured cells expressing the core protein, it has been demonstrated that the core protein interacts with the PPARα-RXRα heterodimer and enhances the transcriptional activation mediated by PPARα regardless of the presence or absence of its ligands.[31] Since PPARα is ubiquitinated and degraded *via* the proteasome pathway,[38] it may be postulated that HCV core protein directly or indirectly influences the degradation pathway. It has been reported that the core protein binds to the proteasome activator PA28γ[39] which is known to combine with steroid receptor coactivator-3 and to accelerate its degradation.[40] Another possible mechanism is an increase in NEFAs in hepatocyte nuclei. The PPARα activation induced by the core protein enhances the expression of L-FABP,[30] which serves as a transporter of NEFAs into nuclei. Indeed, real-time confocal and multiphoton laser scanning microscopy has shown that L-FABP expression significantly increased the total uptake of medium- and long-chain fluorescent fatty acids into the nuclei of living cells.[41] Thus, increased L-FABP expression may facilitate the shuttling of NEFAs into hepatocyte nuclei for donating NEFAs to PPARα, leading to PPARα activation and further increase in L-FABP expression. Moreover, the binding of ligands causes conformational alternation of PPARα[42] and further stabilizes it in nuclei,[32] resulting in synergistic PPARα activation. Therefore, these findings concerning spontaneous and persistent PPARα activation induced by the core protein enable us to partially explain the precise molecular mechanism of hepatocarcinogenesis in HCV core gene transgenic mice.

The results obtained from the current study are consistent with the findings observed in chronically HCV-infected patients in several ways. That is, like the transgenic mice in the present study, chronically HCV-infected patients have been reported to show accelerated hepatocyte proliferation,[43] an increase in CDK4, cyclin D1 and E, PCNA, c-Myc and c-Fos,[34–37] and multicentric appearance of HCC.[44] Furthermore, it has been reported that a massive proliferation of peroxisomes was found in human non-tumorous liver tissue adjacent to HCC.[45] Thus the earlier findings, including the unique function of HCV core protein *in vivo* and the diverse and significant roles of PPARα, may help to partially understand the onset and development of HCC in patients with chronic HCV infection. It has been demonstrated that the function of hepatic PPARα was impaired in patients with chronic HCV infection,[46] which is different from our results. Since HCC had not yet developed in the patients in the report, this discrepancy might derive from differences in the stage of the hepatocarcinogenic process.

The interpretation based on persistent activation of PPARα pertains to only one possible mechanism of hepatocarcinogenesis induced by the effects of HCV core protein. We cannot rule out the presence of other mechanisms. The exact relationship between PPARα activation and hepatocarcinogenesis may be elucidated by additional experiments in which PPARα activation is continuously inhibited in the same transgenic mice. Furthermore, the exact relationship may be confirmed when PPARα-null mice bearing the core protein gene do not represent development of HCC.

In conclusion, we demonstrated for the first time that spontaneous, persistent, age-dependent and heterogeneous activation of PPARα occurred in HCV core protein transgenic mice and caused continuous enhancement of hepatocyte proliferation, which may have contributed to the age-dependent and multicentric hepatocarcinogenesis observed in these mice. In addition, we observed nuclear stabilization of PPARα and an increase in NEFAs in the hepatocyte nuclei of the transgenic mice, which may have resulted in the HCV core protein-specific PPARα activation.

References

1. Kiyosawa K, Tanaka E, Sodeyama T. Hepatitis C virus and hepatocellular carcinoma. In: Reesink HW, ed. Hepatitis C virus: Current Studies in Hematology & Blood Transfusion, vol. 62. Basel: Karger, 1998.161–180.
2. Saito I, Miyamura T, Ohbayashi A, Harada H, Katayama T, Kikuchi S, Watanabe Y, Koi S, Onji M, Ohta Y, Choo QL, Houghton M, et al. Hepatitis C virus infection is associated with the development of hepatocellular carcinoma. Proc Natl Acad Sci USA 1990;87:6547–49.
3. Tanaka Y, Hanada K, Mizokami M, Yeo AE, Shih JW, Gojobori T, Alter HJ. A comparison of the molecular clock of hepatitis C virus in the United States and Japan predicts that hepatocellular carcinoma incidence in the United States will increase over the next two decades. Proc Natl Acad Sci USA 2002;99:15584–89.
4. Kiyosawa K, Umemura T, Ichijo T, Matsumoto A, Yoshizawa K, Gad A, Tanaka E. Hepatocellular carcinoma: recent trends in Japan. Gastroenterology 2004;127:S17–S26.
5. Watashi K, Shimotohno K. The roles of hepatitis C virus proteins in modulation of cellular functions: a novel action mechanism of the HCV core protein on gene regulation by nuclear hormone receptors. Cancer Sci 2003;94:937–43.
6. Ray RB, Lagging LM, Meyer K, Ray R. Hepatitis C virus core protein cooperates with *ras* and transforms primary rat embryo fibroblasts to tumorigenic phenotype. J Virol 1996;70:4438–43.
7. Ray RB, Meyer K, Ray R. Suppression of apoptotic cell death by hepatitis C virus core protein. Virology 1996;226:176–82.
8. McLauchlan J. Properties of the hepatitis C virus core protein: a structural protein that modulates cellular processes. J Viral Hepat 2000; 7:2–14.
9. Tellinghuisen TL, Rice CM. Interaction between hepatitis C virus proteins and host cell factors. Curr Opin Microbiol 2002;5:419–27.
10. Moriya K, Yotsuyanagi H, Shintani Y, Fujie H, Ishibashi K, Matsuura Y, Miyamura T, Koike K. Hepatitis C virus core protein induces hepatic steatosis in transgenic mice. J Gen Virol 1997;78:1527–31.
11. Moriya K, Fujie H, Shintani Y, Yotsuyanagi H, Tsutsumi T, Ishibashi K, Matsuura Y, Kimura S, Miyamura T, Koike K. The core protein of hepatitis C virus induces hepatocellular carcinoma in transgenic mice. Nat Med 1998;4:1065–7.
12. Moriya K, Nakagawa K, Santa T, Shintani Y, Fujie H, Miyoshi H, Tsutsumi T, Miyazawa T, Ishibashi K, Horie T, Imai K, Todoroki T, et al. Oxidative stress in the absence of inflammation in a mouse model for hepatitis C virus-associated hepatocarcinogenesis. Cancer Res 2001;61:4365–70.
13. Sherr CJ. Cancer cell cycles. Science 1996;274:1672–7.
14. Vousden KH, Evan GI. Proliferation, cell cycle and apoptosis in cancer. Nature 2001;411:342–8.
15. Donato MF, Arosio E, Del Ninno E, Ronchi G, Lampertico P, Morabito A, Balestrieri MR, Colombo M. High rates of hepatocellular carcinoma in cirrhotic patients with high liver cell proliferative activity. Hepatology 2001;34:523–8.
16. Yasui K, Wakita T, Tsukiyama-Kohara K, Funahashi S-I, Ichikawa M, Kajita T, Moradpour D, Wands JR, Kohara M. The native form and maturation process of hepatitis C virus core protein. J Virol 1998;72:6048–55.
17. Aoyama T, Peters JM, Iritani N, Nakajima T, Furihata K, Hashimoto T, Gonzalez FJ. Altered constitutive expression of fatty acid-metabo-

lizing enzymes in mice lacking the peroxisome proliferator-activated receptor α (PPARα). J Biol Chem 1998;273:5678–84.
18. Lee SS, Pineau T, Drago J, Lee EJ, Owens JW, Kroetz DL, Fernandez-Salguero PM, Westphal H, Gonzalez FJ. Targeted disruption of the α isoform of the peroxisome proliferator-activated receptor gene in mice results in abolishment of the pleiotropic effects of peroxisome proliferators. Mol Cell Biol 1995;15:3012–22.
19. Peters JM, Aoyama T, Cattley RC, Nobumitsu U, Hashimoto T, Gonzalez FJ. Role of peroxisome proliferator-activated receptor α in altered cell cycle regulation in mouse liver. Carcinogenesis 1998; 19:1989–94.
20. Ni R, Tomita Y, Matsuda K, Ichihara A, Ishimura K, Ogasawara J, Nagata S. Fas-mediated apoptosis in primary cultured mouse hepatocytes. Exp Cell Res 1994;215:332–7.
21. Harada S, Watanabe Y, Takeuchi K, Suzuki T, Katayama T, Takebe Y, Saito I, Miyamura T. Expression of processed core protein of hepatitis C virus in mammalian cells. J Virol 1991;65:3015–21.
22. Novikoff AB, Goldfischer S. Visualization of peroxisomes (microbodies) and mitochondria with diaminobenzidine. J Histochem Cytochem 1969;17:675–80.
23. Gurtu V, Kain SR, Zhang G. Fluorometric and colorimetric detection of caspase activity associated with apoptosis. Anal Biochem 1997; 251:98–102.
24. Folch J, Lees M, Sloane Stanley GH. A simple method for the isolation and purification of total lipids from animal tissues. J Biol Chem 1957;226:497–509.
25. Furutani T, Hino K, Okuda M, Gondo T, Nishina S, Kitase A, Korenaga M, Xiao SY, Weinman SA, Lemon SM, Sakaida I, Okita K. Hepatic iron overload induces hepatocellular carcinoma in transgenic mice expressing the hepatitis C virus polyprotein. Gastroenterology 2006;130:2087–98.
26. Cherkaoui-Malki M, Lone YC, Corral-Debrinski M, Latruffe N. Differential proto-oncogene mRNA induction from rats treated with peroxisome proliferators. Biochem Biophys Res Commun 1990; 173:855–61.
27. Ledwith BJ, Johnson TE, Wagner LK, Pauley CJ, Manam S, Galloway SM, Nichols WW. Growth regulation by peroxisome proliferators: opposing activities in early and late G1. Cancer Res 1996; 56:3257–64.
28. Rininger JA, Goldsworthy TL, Babishi JG. Time course comparison of cell-cycle protein expression following partial hepatectomy and WY14,643-induced hepatic cell proliferation in F344 rats. Carcinogenesis 1997;18:935–41.
29. Peters JM, Cheung C, Gonzalez FJ. Peroxisome proliferator-activated receptor-α and liver cancer: where do we stand? J Mol Med 2005; 83:774–85.
30. Mandard S, Muller M, Kersten S. Peroxisome proliferator-activated receptor α target genes. Cell Mol Life Sci 2004;61:393–416.
31. Tsutsumi T, Suzuki T, Shimoike T, Suzuki R, Moriya K, Shintani Y, Fujie H, Matsuura Y, Koike K, Miyamura T. Interacton of hepatitis C virus core protein with retinoid X receptor α modulates its transcriptional activity. Hepatology 2002;35:937–46.
32. Tanaka N, Hora K, Makishima H, Kamijo Y, Kiyosawa K, Gonzalez FJ, Aoyama T. In vivo stabilization of nuclear retinoid X receptor α in the presence of peroxisome proliferator-activated receptor α. FEBS Lett 2003;543:120–4.
33. Desvergne B, Wahli W. Peroxisome proliferator-activated receptors: nuclear control of metabolism. Endocr Rev 1999;20:649–88.
34. Ito Y, Sasaki Y, Horimoto M, Wada S, Tanaka Y, Kasahara A, Ueki T, Hirano T, Yamamoto H, Fujimoto J, Okamoto E, Hayashi N, et al. Activation of mitogen-activated protein kinases/extracellular signal-regulated kinases in human hepatocellular carcinoma. Hepatology 1998;27:951–8.
35. Masahi T, Shiratori Y, Rengifo W, Igarashi K, Yamagata M, Kurokohchi K, Uchida N, Miyauchi Y, Yoshiji H, Watanabe S, Omata M, Kuriyama S. Cyclins and cyclin-dependent kinases: comparative study of hepatocellular carcinoma versus cirrhosis. Hepatology 2003;37:534–43.
36. Nardone G, Romano M, Calabro A, Pedone PV, de Sio I, Persico M, Budillon G, Bruni CB, Riccio A, Zarrilli R. Activation of fetal promoters of insulin-like growth factors II gene in hepatitis C virus-related chronic hepatitis, cirrhosis, and hepatocellular carcinoma. Hepatology 1996;23:1304–12.
37. Kawate S, Fukusato T, Ohwada S, Watanuki A, Morishita Y. Amplification of *c-myc* in hepatocellular carcinoma: correlation with clinicopathologic features, proliferative activity and p53 overexpression. Oncology 1999;57:157–63.
38. Genini D, Catapano CV. Control of peroxisome proliferator-activated receptor fate by the ubiquitin-proteasome system. J Recept Signal Transduct Res 2006;26:679–92.
39. Moriishi K Okabayashi T, Nakai K, Moriya K, Koike K, Murata S, Chiba T, Tanaka K, Suzuki R, Suzuki T, Miyamura T, Matsuura Y. Proteasome activator PA28γ-dependent nuclear retention and degradation of hepatitis C virus core protein. J Virol 2003;77:10237–49.
40. Li X, Lonard D, Jung SY, Malovannaya A, Feng Q, Qin J, Tsai SY, Tsai M, O'Malley BW. The SRC-3/AIB1 coactivator is degraded in a ubiquitin- and ATP-independent manner by the REGγ proteasome. Cell 2006;124:381–92.
41. Huang H, Starodub O, McIntosh A, Kier AB, Schroeder F. Liver fatty acid-binding protein targets fatty acids to the nucleus. Real time confocal and multiphoton fluorescence imaging in living cells. J Biol Chem 2002;277:29139–51.
42. Dowell P, Peterson VJ, Zabriskie TM, Leid M. Ligand-induced peroxisome proliferator-activated receptor α conformational change. J Biol Chem 1997;272:2013–20.
43. Farinati F, Cardin R, Fiorentino M, D'Errico A, Grigioni W, Cecchetto A, Naccarato R. Imbalance between cytoproliferation and apoptosis in hepatitis C virus related chronic liver disease. J Viral Hepat 2001;8:34–40.
44. Oikawa T, Ojima H, Yamasaki S, Takayama T, Hirohashi S, Sakamoto M. Multistep and multicentric development of hepatocellular carcinoma: histological analysis of 980 resected nodules. J Hepatol 2005;42:225–9.
45. Litwin JA, Beier K, Volkl A, Hofmann WJ, Fahimi HD. Immunocytochemical investigation of catalase and peroxisomal lipid β-oxidation enzymes in human hepatocellular tumors and liver cirrhosis. Virchows Arch 1999;435:486–95.
46. Dharancy S, Malapel M, Perlemuter G, Roskams T, Cheng Y, Dubuquoy L, Podevin P, Conti F, Canva V, Philippe D, Gambiez L, Mathurin P, et al. Impaired expression of the peroxisome proliferator-activated receptor α during hepatitis C virus infection. Gastroenterology 2005;128:334–2.

PPARα activation is essential for HCV core protein–induced hepatic steatosis and hepatocellular carcinoma in mice

Naoki Tanaka,[1,2] Kyoji Moriya,[3] Kendo Kiyosawa,[2] Kazuhiko Koike,[3] Frank J. Gonzalez,[4] and Toshifumi Aoyama[1]

[1]Department of Metabolic Regulation, Institute on Aging and Adaptation, Shinshu University Graduate School of Medicine, Matsumoto, Nagano, Japan.
[2]Division of Gastroenterology, Department of Internal Medicine, Shinshu University School of Medicine, Matsumoto, Nagano, Japan.
[3]Department of Infectious Diseases, Internal Medicine, Graduate School of Medicine, University of Tokyo, Tokyo, Japan.
[4]Laboratory of Metabolism, National Cancer Institute, NIH, Bethesda, Maryland, USA.

Transgenic mice expressing HCV core protein develop hepatic steatosis and hepatocellular carcinoma (HCC), but the mechanism underlying this process remains unclear. Because PPARα is a central regulator of triglyceride homeostasis and mediates hepatocarcinogenesis in rodents, we determined whether PPARα contributes to HCV core protein–induced diseases. We generated PPARα-homozygous, -heterozygous, and -null mice with liver-specific transgenic expression of the core protein gene (*Ppara*$^{+/+}$:HCVcpTg, *Ppara*$^{+/-}$:HCVcpTg, and *Ppara*$^{-/-}$:HCVcpTg mice. Severe steatosis was unexpectedly observed only in *Ppara*$^{+/+}$:HCVcpTg mice, which resulted from enhanced fatty acid uptake and decreased mitochondrial β-oxidation due to breakdown of mitochondrial outer membranes. Interestingly, HCC developed in approximately 35% of 24-month-old *Ppara*$^{+/+}$:HCVcpTg mice, but tumors were not observed in the other genotypes. These phenomena were found to be closely associated with sustained PPARα activation. In *Ppara*$^{+/-}$:HCVcpTg mice, PPARα activation and the related changes did not occur despite the presence of a functional *Ppara* allele. However, long-term treatment of these mice with clofibrate, a PPARα activator, induced HCC with mitochondrial abnormalities and hepatic steatosis. Thus, our results indicate that persistent activation of PPARα is essential for the pathogenesis of hepatic steatosis and HCC induced by HCV infection.

Introduction

HCV is one of the major causes of chronic hepatitis, whereas patients with persistent HCV infection have a high incidence of hepatocellular carcinoma (HCC) (1, 2). Occurrence of HCC associated with chronic HCV infection has increased over the past 2 decades (3–5), and chronic HCV infection is recognized as a serious debilitating disease. However, the mechanism in which chronic HCV infection mediates hepatocarcinogenesis remains unclear.

HCV core protein was shown to have oncogenic potential (6). To examine how HCV core protein participates in HCV-related hepatocarcinogenesis, transgenic mouse lines were established in which HCV core protein is expressed constitutively in liver at cellular levels similar to those found in chronic HCV-infected patients (7). These mice exhibited hepatic steatosis (7) and insulin resistance (8) as early as 3 months of age; on further aging, these symptoms worsened and hepatic adenomas developed in approximately 30% of mice between 16 and 18 months of age (9). Finally, HCC was found within hepatic adenomas in a classic "nodule-in-nodule" pathology (9). Interestingly, no hepatic inflammation or fibrosis was found in these mice throughout the course of HCC development (9), which suggested that the HCV core protein itself induces hepatic steatosis and HCC independently of hepatitis.

Several studies support the contention that hepatic steatosis promotes the development of HCC (10). Epidemiologic data have identified hepatic steatosis as a major accelerating factor of hepatocarcinogenesis in chronic HCV-infected patients (11). Moreover, increases in ROS production that can cause oxidative DNA damage, mitochondrial abnormalities, and accelerated hepatocyte proliferation were observed in the steatotic livers (12–14). Thus, an intriguing possibility has emerged that alteration of fatty acid metabolism in hepatocytes may be central to the pathogenesis of HCC induced by HCV core protein.

PPARs are ligand-activated nuclear receptors belonging to the steroid/thyroid hormone receptor superfamily; 3 isoforms designated as α, β/δ, and γ exist, all of which are involved in lipid homeostasis (15). PPARα regulates constitutive transcription of genes encoding fatty acid–metabolizing enzymes (16) and is associated with the maintenance of fatty acid transport and metabolism, primarily in liver, kidney, and heart. Administration of PPARα agonists, such as the widely prescribed fibrate drugs clofibrate, gemfibrozil, and fenofibrate, ameliorate hyperlipidemia in humans (17) and hepatic steatosis in mice (18).

On the other hand, long-term administration of PPARα ligands to rodents causes accelerated hepatocyte proliferation, increased ROS generation, and development of HCC (19, 20). Disruption of the PPARα gene was shown to prevent the development of HCC caused by long-term exposure to PPARα activators (21). Interestingly, accumulation of fatty acids/triglycerides in hepatocytes

Nonstandard abbreviations used: ACC, acetyl-CoA carboxylase; AOX, acyl-CoA oxidase; CDK, cyclin-dependent kinase; CYP4A1, cytochrome P450 4A1; FAS, fatty acid synthase; FAT, fatty acid translocase; FATP, fatty acid transport protein; HCC, hepatocellular carcinoma; HCVcpTg, HCV core protein–expressing transgenic; L-FABP, liver fatty acid-binding protein; MCAD, medium-chain acyl-CoA dehydrogenase; MTP, microsomal transfer protein; 8-OHdG, 8-hydroxy-2′-deoxyguanosine; PCNA, proliferating cell nuclear antigen; RXRα, retinoid X receptor α.

Conflict of interest: The authors have declared that no conflict of interest exists.

Citation for this article: *J. Clin. Invest.* 118:683–694 (2008). doi:10.1172/JCI33594.

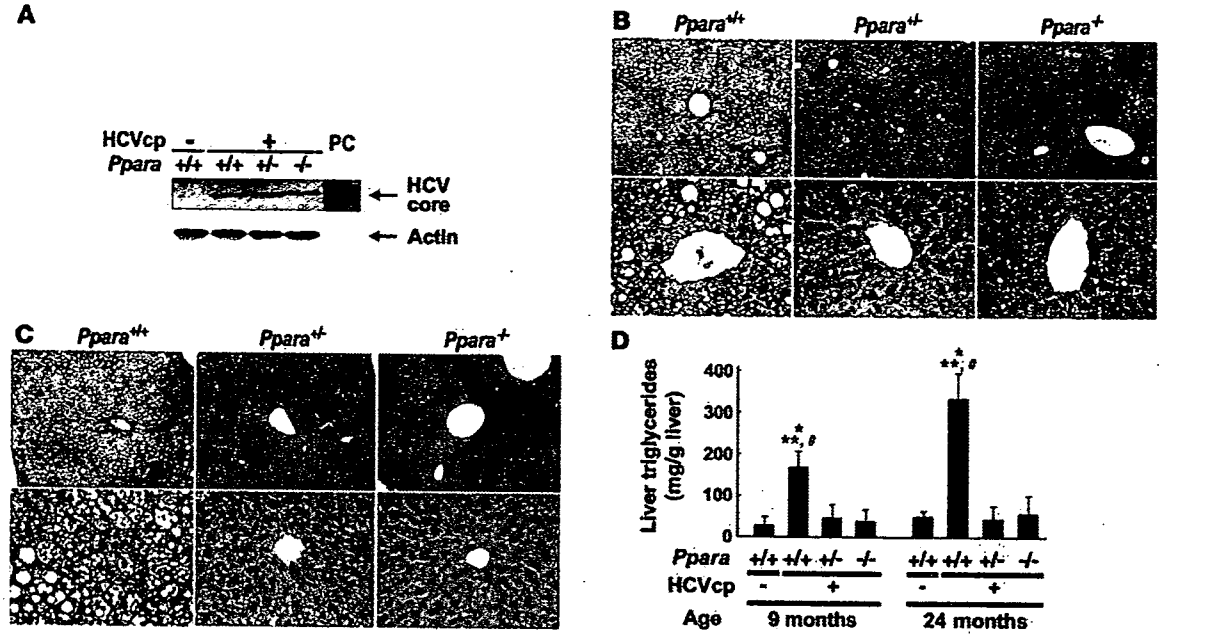

Figure 1

Phenotype changes in transgenic mouse liver. (**A**) Immunoblot analysis of HCV core protein expression in livers of 9-month-old mice. Because no significant individual differences in the same mouse group were found in the preliminary experiments, 10 mg of liver prepared from each mouse ($n = 6$ /group) was mixed and homogenized. Whole-liver lysate (50 μg protein) was loaded in each well. The band of actin was used as the loading control. Results are representative of 4 independent experiments. PC, lysate prepared from COS-1 cells overexpressing HCV core protein as a positive control. (**B**) Histological appearance of hematoxylin- and eosin-stained liver sections from 9-month-old HCVcpTg mice. Upper and lower rows show a lower (×40) and higher (×400) magnification, respectively. Microvesicular and macrovesicular steatosis was found only in *Ppara*$^{+/+}$:HCVcpTg mice. No inflammation or hepatocyte degeneration was evident in any of the genotypes. (**C**) Histological appearance of hematoxylin- and eosin-stained liver sections from 24-month-old HCVcpTg mice. Upper and lower rows show a lower (×40) and higher (×400) magnification, respectively. Hepatic steatosis was marked in *Ppara*$^{+/+}$:HCVcpTg mice, but not in other mice. Hepatic inflammation, fibrosis, and hepatocyte degeneration were not observed. In *Ppara*$^{+/-}$:HCVcpTg and *Ppara*$^{-/-}$:HCVcpTg mice, dysplastic hepatocytes and precancerous lesions were not detected throughout the entire liver. (**D**) Content of liver triglycerides. Results are expressed as the mean ± SD ($n = 6$/group) and compared between genotypes at the same age. $^{*}P < 0.05$ compared with *Ppara*$^{+/+}$ nontransgenic mice; $^{**}P < 0.05$ compared with *Ppara*$^{+/-}$:HCVcpTg mice; $^{\#}P < 0.05$ compared with *Ppara*$^{-/-}$:HCVcpTg mice.

could lead to continuous PPARα activation because of the presence of fatty acid metabolites that serve as natural PPARα ligands. For example, mice lacking expression of the peroxisomal acyl-CoA oxidase (AOX) gene showed massive accumulation of very-long-chain fatty acids in hepatocytes, severe microvesicular steatosis, chronic PPARα activation, and development of hepatic adenoma and HCC by 15 months of age (22). These results suggest a strong contribution of activated PPARα to liver tumorigenesis.

On the basis of several lines of evidence, we hypothesized that PPARα might contribute to hepatocarcinogenesis in HCV core protein–expressing transgenic (HCVcpTg) mice. To explore this possibility, PPARα-homozygous (*Ppara*$^{+/+}$), PPARα-heterozygous (*Ppara*$^{+/-}$), and PPARα-null (*Ppara*$^{-/-}$) mice bearing the HCV core protein gene, designated *Ppara*$^{+/+}$:HCVcpTg, *Ppara*$^{+/-}$:HCVcpTg, and *Ppara*$^{-/-}$:HCVcpTg mice, were generated, and phenotypic changes were examined. Surprisingly, we found that severe hepatic steatosis and HCC induced by HCV core protein developed only in *Ppara*$^{+/+}$ mice, which were related to persistent PPARα activation.

Results

Expression of HCV core protein in transgenic mice. *Ppara*$^{-/-}$:HCVcpTg and *Ppara*$^{+/-}$:HCVcpTg mice appeared healthy, and body weight in both genotypes was similar to that of *Ppara*$^{+/+}$:HCVcpTg and *Ppara*$^{+/+}$ mice without the transgene. When hepatic expression of HCV core protein in 9-month-old transgenic mice was examined by immunoblot analysis, it was similar among *Ppara*$^{+/+}$:HCVcpTg, *Ppara*$^{+/-}$:HCVcpTg, and *Ppara*$^{-/-}$:HCVcpTg mice (Figure 1A) and was also similar to expression in HCVcpTg mice reported previously (7, 9). Age and sex had only a minor influence on the hepatic expression of HCV core protein.

Requirement of homozygous PPARα for the development of hepatic steatosis in transgenic mice. Livers of 9-month-old male HCVcpTg mice with or without the *Ppara* allele were examined. Those of *Ppara*$^{+/+}$:HCVcpTg mice were soft, slightly enlarged, and light in color and histologically showed macrovesicular and microvesicular steatosis with no apparent inflammation or hepatocyte necrosis (Figure 1B), in agreement with previous reports (7, 9). Biochemical analysis of liver extracts showed marked hepatic accumulation of triglycerides (Figure 1D). In contrast, livers of 9-month-old *Ppara*$^{+/-}$:HCVcpTg and *Ppara*$^{-/-}$:HCVcpTg mice showed neither histological abnormalities nor accumulation of triglycerides (Figure 1, B and D). Hepatic levels of free fatty acids in *Ppara*$^{+/+}$:HCVcpTg mice were approximately 3 times those in *Ppara*$^{+/-}$:HCVcpTg and *Ppara*$^{-/-}$:HCVcpTg mice or *Ppara*$^{+/+}$ mice not expressing the HCV core protein.

In 24-month-old *Ppara*$^{+/+}$:HCVcpTg mice, hepatic steatosis was found (Figure 1C), and the hepatic levels of triglycerides were further increased (Figure 1D). Apparent inflammation, hepatocyte

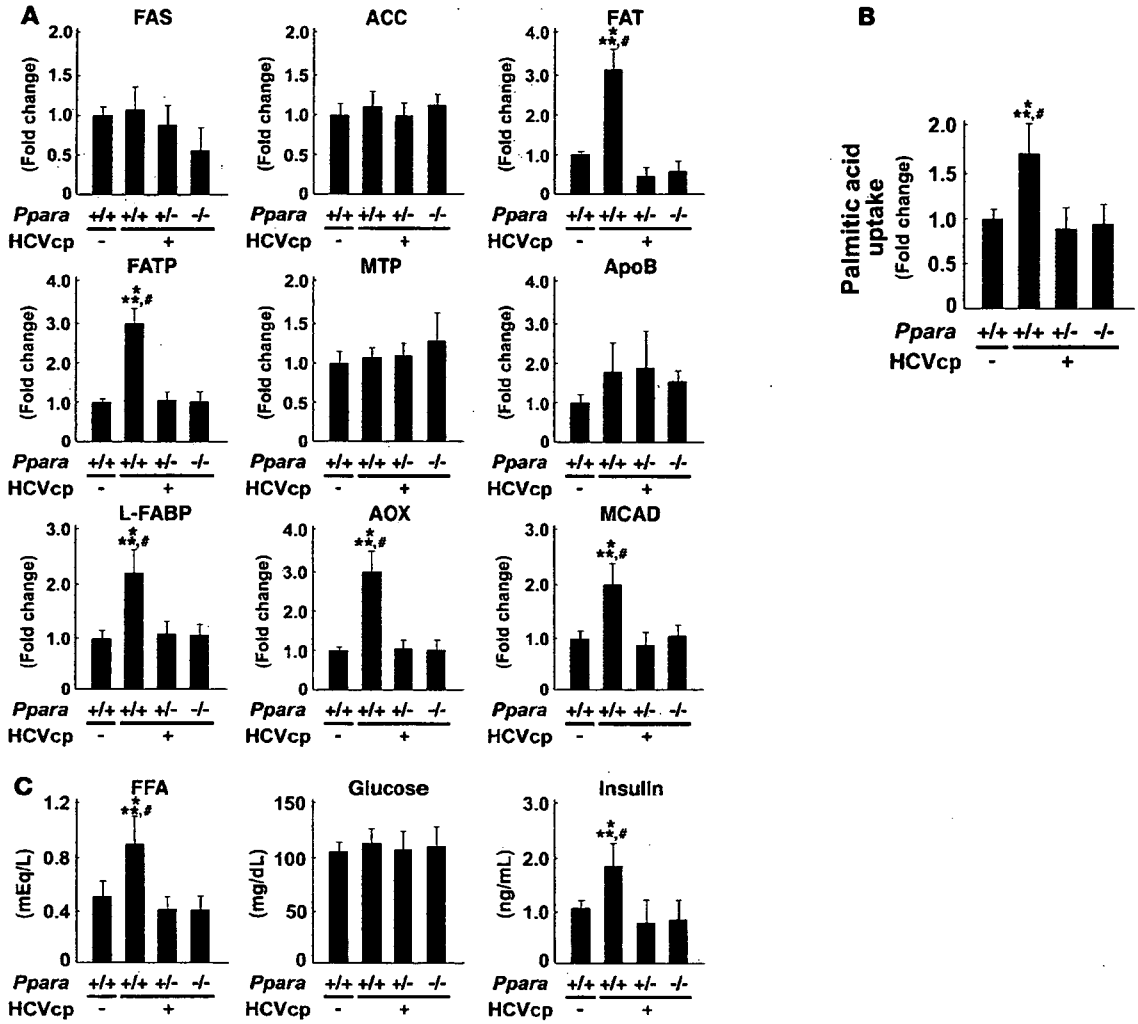

Figure 2

Analyses of factors associated with hepatic fatty acid and triglyceride metabolism. (**A**) Expression of genes associated with fatty acid and triglyceride metabolism in 9-month-old mouse livers. Total RNA was extracted from each mouse liver, and mRNA levels were determined by RT-PCR. mRNA levels were normalized by those of GAPDH and subsequently normalized by those in *Ppara*$^{+/+}$ nontransgenic mice. Results are expressed as the mean ± SD (n = 6/group). *P < 0.05 compared with *Ppara*$^{+/+}$ nontransgenic mice; **P < 0.05 compared with *Ppara*$^{+/-}$:HCVcpTg mice; #P < 0.05 compared with *Ppara*$^{-/-}$:HCVcpTg mice. (**B**) Uptake of fatty acids in 9-month-old mouse livers. Liver slices obtained from 3 mice in each group were incubated in medium containing 0.8 mM [1-^{14}C]palmitic acid for 7 h. Fatty acid uptake ability was estimated by the sum of palmitic acid converted to CO_2 and ketone bodies with that incorporated into total cellular lipids after incubation. The experiment was repeated 3 times. Results were normalized by those of *Ppara*$^{+/+}$ nontransgenic mice and expressed as the mean ± SD. (**C**) Plasma concentrations of free fatty acids, glucose, and insulin. After an overnight fast, blood was obtained from each mouse and the above variables were determined. Results are expressed as the mean ± SD (n = 6/group).

degeneration and necrosis, and fibrosis were not detected. On the other hand, *Ppara*$^{+/-}$:HCVcpTg and *Ppara*$^{-/-}$:HCVcpTg mice showed no steatosis (Figure 1, C and D). These results indicate that hepatic steatosis develops in *Ppara*$^{+/+}$:HCVcpTg mice, but not in *Ppara*$^{+/-}$:HCVcpTg and *Ppara*$^{-/-}$:HCVcpTg mice.

Hepatic fatty acid and triglyceride metabolism in transgenic mice. To investigate the mechanism responsible for the development of severe steatosis in *Ppara*$^{+/+}$:HCVcpTg mice, the expression of genes associated with fatty acid and triglyceride metabolism in the livers of 9-month-old mice was analyzed using the quantitative RT-PCR method. As shown in Figure 2A, the mRNA levels of genes related to de novo lipogenesis (fatty acid synthase [FAS] and acetyl-CoA carboxylase [ACC]) and secretion of VLDL (microsomal transfer protein [MTP] and apoB) were constant in all groups. The mRNA levels of fatty acid translocase (FAT) and fatty acid transport protein (FATP), which are associated with the uptake of fatty acids into hepatocytes, were significantly increased only in *Ppara*$^{+/+}$:HCVcpTg mice, but the mRNA levels of hepatic triglyceride lipase, another contributor to fatty acid uptake, remained unchanged (data not shown). The mRNA levels of liver fatty acid binding protein (L-FABP) were also elevated only in *Ppara*$^{+/+}$:HCVcpTg mice. Surprisingly, the mRNA levels of AOX and medium-chain acyl-CoA

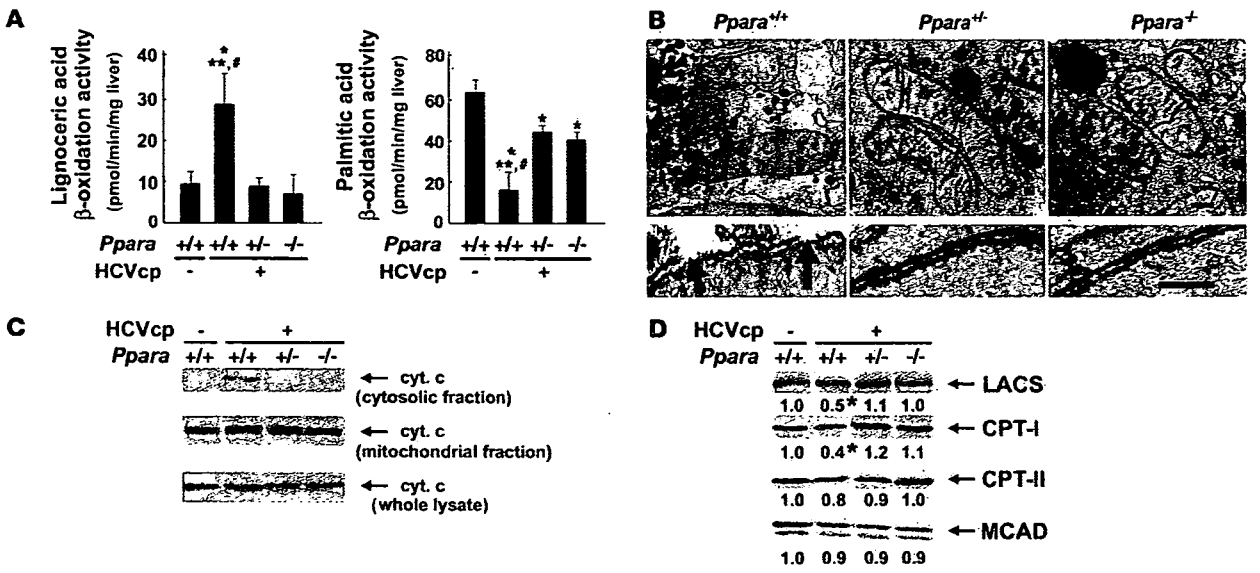

Figure 3

Analyses of mitochondrial abnormalities. (**A**) Lignoceric and palmitic acid β-oxidation activities in 9-month-old mice. Results are expressed as the mean ± SD (n = 6/group). *P < 0.05 compared with *Ppara*$^{+/+}$ nontransgenic mice; **P < 0.05 compared with *Ppara*$^{+/-}$:HCVcpTg mice; $^{\#}P$ < 0.05 compared with *Ppara*$^{-/-}$:HCVcpTg mice. (**B**) Electron microscopic features of hepatic mitochondria of 9-month-old HCVcpTg mice. Upper and lower rows show a lower and higher magnification, respectively. In *Ppara*$^{+/+}$:HCVcpTg mice, some mitochondria showing discontinuance of outer membranes (arrows) and amorphous inner structures were observed. In *Ppara*$^{+/-}$:HCVcpTg and *Ppara*$^{-/-}$:HCVcpTg mice, mitochondria appeared normal; the scale bars represent 200 nm (top) and 30 nm (bottom), respectively. (**C**) Immunoblot analysis of cytochrome *c* in 9-month-old mice. Whole-liver lysate, mitochondrial fraction, or cytosolic fraction (50 μg protein) was loaded in each well. Results are representative of 4 independent experiments. (**D**) Immunoblot analysis of representative mitochondrial β-oxidation enzymes using a mitochondrial fraction prepared from 9-month-old mouse livers. The mitochondrial fraction (20 μg protein) was loaded in each well. Results are representative of 4 independent experiments. The band intensity was quantified densitometrically and normalized by that in *Ppara*$^{+/+}$ nontransgenic mouse. The mean value of the fold changes is shown under the representative band. LACS, long-chain acyl-CoA synthase; CPT, carnitine palmitoyl-CoA transferase.

dehydrogenase (MCAD), a rate-limiting enzymes in the peroxisomal and mitochondrial β-oxidation pathways, respectively, were significantly increased in *Ppara*$^{+/+}$:HCVcpTg mice. When fatty acid uptake ability was measured in fresh liver slices, it was significantly enhanced only in *Ppara*$^{+/+}$:HCVcpTg mice (Figure 2B). Additionally, plasma free fatty acid levels were higher in these mice than in mice in the other groups. Although there were no differences in fasting plasma glucose levels between the groups, hyperinsulinemia was observed only in *Ppara*$^{+/+}$:HCVcpTg mice (Figure 2C), in agreement with the previous observation that significant insulin resistance developed in these mice (8). Similar results were obtained from 24-month-old mice (data not shown). These results combined show that the increased plasma fatty acid levels, which were likely due to enhanced peripheral fatty acid release caused by insulin resistance, and the increase in fatty acid uptake ability are consistent with steatogenesis in *Ppara*$^{+/+}$:HCVcpTg mice.

Decreased mitochondrial β-oxidation in transgenic mice. Although the transcriptional activities of major β-oxidation enzymes were markedly increased, *Ppara*$^{+/+}$:HCVcpTg mice had severe steatosis. To explore this discrepant result, peroxisomal and mitochondrial β-oxidation activities were measured using lignoceric and palmitic acids as substrates, respectively. The lignoceric acid–degrading capacity was increased only in *Ppara*$^{+/+}$:HCVcpTg mice, where it corresponded to an increase in AOX expression. However, the capacity for palmitic acid degradation, which occurs particularly in mitochondria, was significantly lower in *Ppara*$^{+/+}$:HCVcpTg mice than in *Ppara*$^{+/-}$:HCVcpTg and *Ppara*$^{-/-}$:HCVcpTg mice (Figure 3A). Thus, decreased mitochondrial β-oxidation ability was considered to be another important mechanism for the development of steatosis induced by the core protein.

We further evaluated mitochondrial abnormalities. In electron microscopic examination, discontinuous outer membranes (Figure 3B, arrows) and lack of an internal structure were observed in some mitochondria of *Ppara*$^{+/+}$:HCVcpTg mouse livers, in agreement with the previous report (9). However, these abnormalities were not seen in *Ppara*$^{+/-}$:HCVcpTg and *Ppara*$^{-/-}$:HCVcpTg mice (Figure 3B). Immunoblot analysis showed that cytochrome *c*, which is usually localized in the mitochondrial intermembrane space, was present in the cytosolic fractions of *Ppara*$^{+/+}$:HCVcpTg mice (Figure 3C). Moreover, immunoblot analysis using mitochondrial fractions showed that the expression levels of long-chain acyl-CoA synthase and carnitine palmitoyl-CoA transferase-I, which are enzymes indispensable to the initial step of mitochondrial β-oxidation and are localized mainly in mitochondrial outer membranes, were significantly decreased only in *Ppara*$^{+/+}$:HCVcpTg mice (Figure 3D).

Overall, these results suggest that homozygous PPARα is essential to the pathogenesis of hepatic steatosis induced by the HCV core protein, which results from a decrease in mitochondrial fatty acid degradation capacity caused by the breakdown of mitochondrial outer membranes and a disproportionate increase in the uptake of fatty acids. Interestingly, steatosis and the related changes did not occur in *Ppara*$^{+/-}$ and *Ppara*$^{-/-}$ mice expressing the HCV core protein, which suggested that these changes were not caused by the core protein itself.

Table 1
Incidence of HCC in 24-month-old mice

HCV core protein	*Ppara*	Mice (*n*)	Mice with HCC (*n*)	Incidence (%)
–	+/+	20	0	0
–	+/–	18	0	0
–	–/–	20	0	0
+	+/+	17	6	35.3[A]
+	+/–	16	0	0
+	–/–	14	0	0

Mice were killed at 24 months of age for analysis. HCC was diagnosed according to histological findings. [A]$P < 0.05$ compared with *Ppara*$^{+/+}$ nontransgenic mice, $P < 0.05$ compared with *Ppara*$^{+/-}$:HCVcpTg mice, $P < 0.05$ compared with *Ppara*$^{-/-}$:HCVcpTg mice.

Requirement of homozygous PPARα for hepatic tumor development in transgenic mice. At 9 months of age, hepatic nodules were not observed at all in transgenic mice, whereas, at 24 months, approximately 35% of *Ppara*$^{+/+}$:HCVcpTg mice had macroscopically evident hepatic nodules (Table 1). Microscopically, these nodules had the appearance of well-differentiated HCC with trabecular features, which was consistent with the previous report (9). Surprisingly, *Ppara*$^{+/-}$:HCVcpTg and *Ppara*$^{-/-}$:HCVcpTg mice of the same ages developed no evidence of hepatic tumors, despite the expression of HCV core protein at similar levels to those found in *Ppara*$^{+/+}$:HCVcpTg mice (Table 1). Microscopic examination showed that there were no dysplastic cells or precancerous lesions throughout the livers in *Ppara*$^{+/-}$:HCVcpTg and *Ppara*$^{-/-}$:HCVcpTg mice (Figure 1C). These results provide strong evidence that homozygous PPARα is essential for hepatic tumorigenesis induced by HCV core protein.

Increased hepatocyte proliferation only in Ppara$^{+/+}$*:HCVcpTg mice.* Because sustained acceleration of hepatocyte proliferation relative to apoptosis may promote the development of HCC, these opposing processes were quantified in the livers of 24-month-old mice. Both the liver-to-body weight ratio and the number of hepatocytes expressing proliferating cell nuclear antigen (PCNA) were increased only in *Ppara*$^{+/+}$:HCVcpTg mice (Figure 4, A and B). In contrast, the number of TUNEL-positive hepatocytes and the hepatic caspase 3 activity, indicators of hepatocyte apoptosis, remained similar among the 3 mouse strains (Figure 4, C and D). Interestingly, despite the presence of HCV core protein, the amounts of these proliferative and apoptotic markers in *Ppara*$^{+/-}$:HCVcpTg and *Ppara*$^{-/-}$:HCVcpTg mice were similar to those in *Ppara*$^{+/+}$ nontransgenic mice. Expression levels of several proteins, such as protooncogenes (c-Fos and c-Myc), cell-cycle regulators (cyclin D1, cyclin-dependent kinase [CDK] 4, and PCNA), and phosphorylated ERK 1 and 2, all of which are associated with hepatocyte proliferation, were elevated in *Ppara*$^{+/+}$:HCVcpTg mice but not in other genotypes (Figure 4, E and F).

Increased oxidative stress and DNA damage only in Ppara$^{+/+}$*:HCVcpTg mice.* HCV core protein is associated with increased production of ROS (23). Enhanced ROS production induces nuclear DNA damage, which results in the initiation of hepatocarcinogenesis, and can also injure organelles, which can result in disorders in their

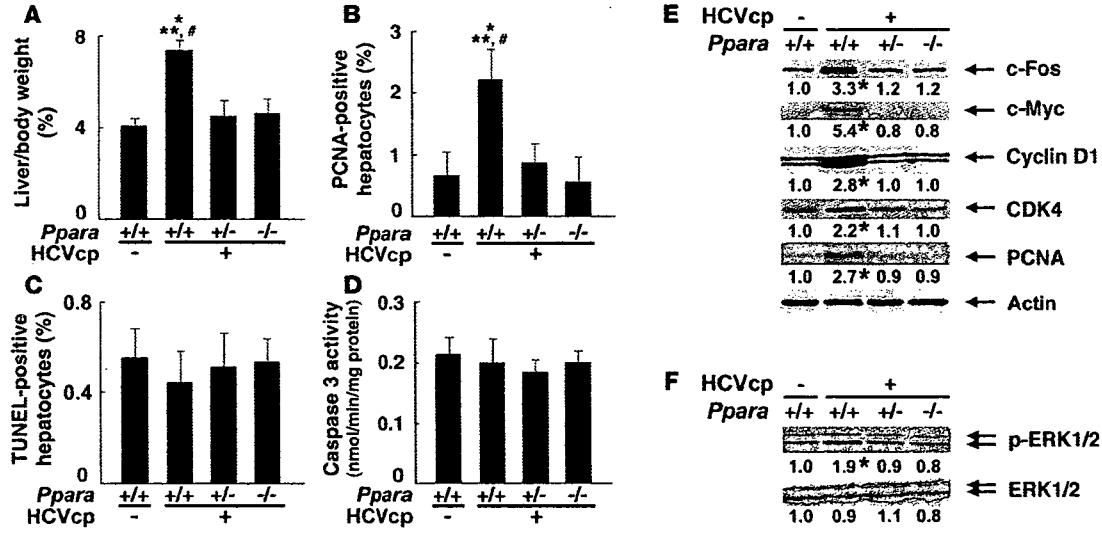

Figure 4
Increased hepatocyte proliferation in *Ppara*$^{+/+}$:HCVcpTg mice at 24 months of age. (**A**) Liver-to-body-weight ratio. Results are expressed as the mean ± SD (n = 6/group). (**B**) Numbers of proliferating hepatocytes. Two thousand hepatocytes were examined in each mouse, and hepatocyte nuclei positive for anti-PCNA antibody were counted. Results are expressed as the mean ± SD (n = 6/group). For **A** and **B**, comparisons are designated as follows: *$P < 0.05$ compared with *Ppara*$^{+/+}$ nontransgenic mice; **$P < 0.05$ compared with *Ppara*$^{+/-}$:HCVcpTg mice; #$P < 0.05$ compared with *Ppara*$^{-/-}$:HCVcpTg mice. (**C**) Numbers of apoptotic hepatocytes. Liver sections were subjected to TUNEL staining, and TUNEL-positive hepatocyte nuclei were counted in 2,000 hepatocytes from each mouse. Results are expressed as the mean ± SD (n = 6/group). (**D**) Caspase 3 activity. Results are expressed as the mean ± SD (n = 6/group). (**E**) Immunoblot analysis of oncogene products and cell cycle regulators. The same sample used in Figure 1A (whole-liver lysate; 50 μg protein) was loaded in each well. The band of actin was used as the loading control. Results are representative of 4 independent experiments. The band intensity was quantified densitometrically, normalized by that of actin, and subsequently normalized by that in *Ppara*$^{+/+}$ nontransgenic mice. The mean value of the fold changes is expressed under each band. (**F**) Immunoblot analysis of phosphorylated ERK1/2 and total ERK1/2. The same samples in Figure 4E (50 μg protein) were used.

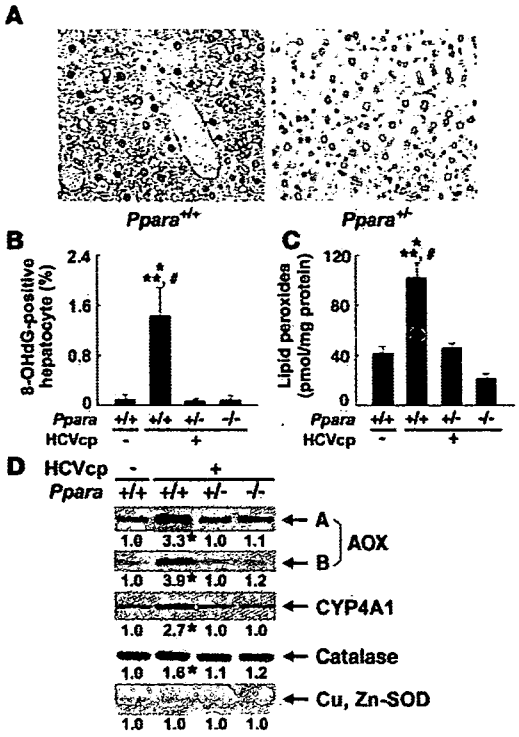

Figure 5

Increased oxidative stress and DNA damage in *Ppara*$^{+/+}$:HCVcpTg mice at 24 months of age. (**A**) Immunohistochemical staining using antibody against 8-OHdG. In *Ppara*$^{+/+}$:HCVcpTg mice, some steatotic hepatocytes were positive for 8-OHdG. Original magnification, ×400. (**B**) Numbers of 8-OHdG–positive hepatocytes. Hepatocyte nuclei stained with anti-8-OHdG antibody were counted in 2,000 hepatocytes of each mouse. Results are expressed as the mean ± SD (n = 6/group). (**C**) Hepatic content of lipid peroxides. Results are expressed as the mean ± SD (n = 6 /group). $^*P < 0.05$ compared with *Ppara*$^{+/+}$ nontransgenic mice; $^{**}P < 0.05$ compared with *Ppara*$^{+/-}$:HCVcpTg mice; $^{\#}P < 0.05$ compared with *Ppara*$^{-/-}$:HCVcpTg mice. (**D**) Immunoblot analysis of AOX, CYP4A1, catalase, and Cu, Zn-SOD. The whole-liver lysate used in the experiment in Figure 4E (20 μg protein for AOX and CYP4A1 and 50 μg for others) was loaded in each lane. The band of actin was used as the loading control. Results are representative of 4 independent experiments. **A** and **B** indicate full-length and truncated AOX, respectively. The band intensity was quantified densitometrically, normalized by that of actin, and subsequently normalized by that in *Ppara*$^{+/+}$ nontransgenic mice. The mean value of the fold changes is expressed under each band. $^*P < 0.05$ compared with *Ppara*$^{+/+}$ nontransgenic mice.

function. The number of hepatocytes positive for 8-hydroxy-2'-deoxyguanosine (8-OHdG), an indicator of oxidative damage to nuclear DNA, was increased only in 24-month-old *Ppara*$^{+/+}$:HCVcpTg mice (Figure 5, A and B). Lipid peroxides were slightly increased in the livers of 9-month-old *Ppara*$^{+/+}$:HCVcpTg mice (data not shown) and were more abundant in the livers of 24-month-old *Ppara*$^{+/+}$:HCVcpTg mice than in those of *Ppara*$^{+/-}$:HCVcpTg and *Ppara*$^{-/-}$:HCVcpTg mice or *Ppara*$^{+/+}$ nontransgenic mice (Figure 5C). Expression of typical ROS-generating enzymes (AOX and cytochrome P450 4A1 [CYP4A1]) and ROS-eliminating enzymes (catalase and Cu, Zn-SOD) was examined. Immunoblot analysis showed marked increases in the expression of AOX and CYP4A1 and mild increases in that of catalase only in *Ppara*$^{+/+}$:HCVcpTg mice. No changes in Cu, Zn-SOD were found in the subgroups of transgenic mice (Figure 5D). These results suggest that enhanced oxidative stress causes damage in nuclear DNA and probably in mitochondria in the *Ppara*$^{+/+}$:HCVcpTg mice.

Persistent and spontaneous PPARα activation in Ppara$^{+/+}$*:HCVcpTg mice.* Liver tumorigenesis induced by long-term exposure to peroxisome proliferators and the related changes, such as sustained hepatocyte proliferation and increased oxidative stress, are associated with persistent PPARα activation (19–21). To examine the activation of PPARα, we quantified the level of PPARα mRNA, which is induced by PPARα activation (24, 25). PPARα mRNA levels were higher in 9-month-old *Ppara*$^{+/+}$:HCVcpTg mice than in *Ppara*$^{+/+}$ nontransgenic mice (Figure 6A). These increases were more pronounced at 24 months of age. However, there were no differences in PPARα mRNA levels between *Ppara*$^{+/-}$:HCVcpTg and *Ppara*$^{+/-}$ nontransgenic mice at either 9 or 24 months of age. The expression levels of typical PPARα target genes (16, 25, 26) – such as FAT, FATP, L-FABP, AOX, and MCAD (Figure 2); c-Myc, cyclin D1, CDK4, and PCNA (Figure 4); and CYP4A1 (Figure 5) – were simultaneously and synchronously increased in *Ppara*$^{+/+}$:HCVcpTg mice, but not in *Ppara*$^{+/-}$:HCVcpTg or *Ppara*$^{-/-}$:HCVcpTg mice. These results confirm that persistent activation of PPARα occurs only in *Ppara*$^{+/+}$:HCVcpTg mice. Various changes observed in *Ppara*$^{+/+}$:HCVcpTg mice, i.e., increased fatty acid uptake, mitochondrial abnormalities, steatosis, ROS overproduction, accelerated hepatocyte proliferation, and hepatocarcinogenesis, were considered to be closely linked with sustained PPARα activation.

Nuclear PPARα content. The results described above suggest that persistent PPARα activation is critical to the steatogenesis and hepatocarcinogenesis induced by the HCV core protein. A question arises as to why *Ppara*$^{+/-}$:HCVcpTg mice with an active *Ppara* allele do not exhibit the hallmarks of PPARα activation and do not develop HCC. To address this issue, the nuclear PPARα content was analyzed. Immunoblot analysis for PPARα showed that the amount of nuclear PPARα protein in *Ppara*$^{+/+}$:HCVcpTg mice was approximately 2- to 3-fold that of *Ppara*$^{+/+}$ nontransgenic mice, which was disproportionate to the higher PPARα mRNA levels (approximately 1.2- to 1.6-fold) (Figure 6, A and B). The level of nuclear PPARα in *Ppara*$^{+/-}$:HCVcpTg mice was significantly lower than that in *Ppara*$^{+/+}$:HCVcpTg mice and was similar to that in *Ppara*$^{+/+}$ nontransgenic mice (Figure 6B). Thus, the lower amount of nuclear PPARα in *Ppara*$^{+/-}$:HCVcpTg mice than in *Ppara*$^{+/+}$:HCVcpTg mice might have heightened the threshold of expression required for long-term spontaneous PPARα activation.

The degree of an increase in nuclear PPARα levels was evidently higher than the degree of an increase in PPARα mRNA levels in HCVcpTg mice (Figure 6, A and B). To investigate this disparity, the stability of nuclear PPARα was evaluated by pulse-chase experiments using isolated hepatocytes obtained from these mice. The half-life of nuclear PPARα was significantly longer ($P < 0.05$) in *Ppara*$^{+/+}$:HCVcpTg mice (11.5 ± 2.3 h) than in *Ppara*$^{+/+}$ nontransgenic mice (5.8 ± 1.4 h) (Figure 6C). The half-life of nuclear PPARα in *Ppara*$^{+/-}$:HCVcpTg mice tended to be prolonged compared with that in *Ppara*$^{+/-}$ nontransgenic mice (Figure 6C). These results suggest that the stability of nuclear PPARα was increased as a result of HCV core protein expression. Because it is known that the core protein interacts with retinoid X receptor α (RXRα) (27) and that

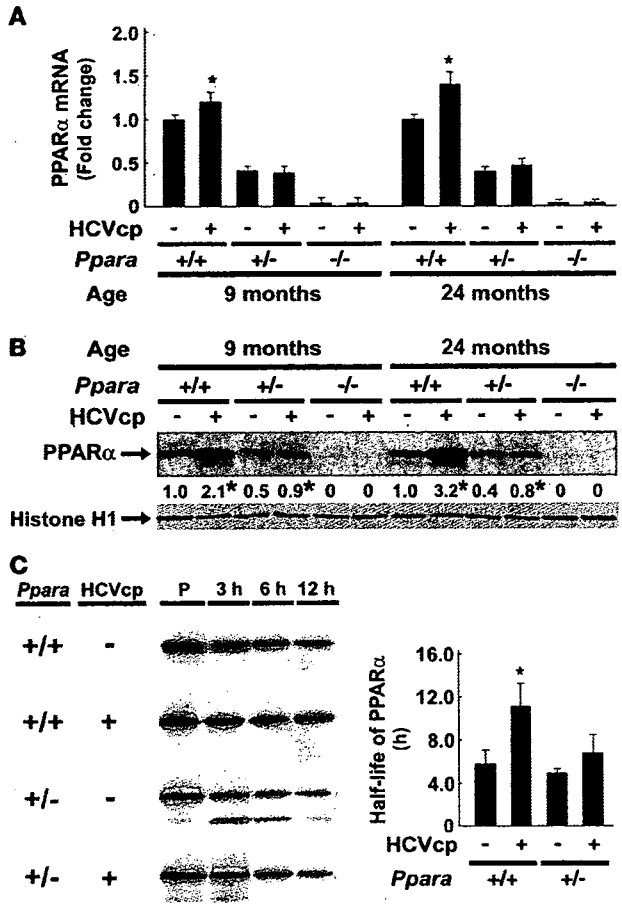

Figure 6
Persistent PPARα activation in *Ppara*$^{+/+}$:HCVcpTg mice. (**A**) PPARα mRNA levels. Total RNA was prepared from each mouse, and PPARα mRNA levels were determined by RT-PCR, normalized by those of GAPDH, and subsequently normalized by those of 9-month-old *Ppara*$^{+/+}$ nontransgenic mice. Results are expressed as the mean ± SD (n = 6 /group). (**B**) Immunoblot analysis of nuclear PPARα. The nuclear fraction obtained from each mouse (100 μg protein) was loaded in each well. The band of histone H1 was used as the loading control. Results are representative of 6 independent experiments. The band intensity was quantified densitometrically, normalized by that of histone H1, and subsequently normalized by that in 9-month-old *Ppara*$^{+/+}$ nontransgenic mice. The mean value is expressed under each band. *P < 0.05 compared with nontransgenic mice of the same age and *Ppara* genotype. (**C**) Pulse-chase experiments for 3, 6, and 12 h and pulse-label (P) experiments for nuclear PPARα using isolated mouse hepatocytes. Left: labeled PPARα bands on x-ray film. Pulse-label and pulse-chase experiments were performed as described in Methods. Results are representative of 4 independent experiments. Right: half-life of PPARα. The band intensity was measured densitometrically and subsequently normalized by that of the pulse-label experiments. The percentage of the band intensity was plotted, and the half-life of PPARα was calculated. Results obtained from 4 independent experiments are expressed as the mean ± SD. *P < 0.05 compared with nontransgenic mice in the same *Ppara* genotype.

PPARα influences the stability of RXRα (28), it is plausible that the core protein would affect its action in nuclei through an interaction with the PPARα-RXRα heterodimer and stabilization of PPARα.

Development of hepatic steatosis and HCC with long-term clofibrate treatment in Ppara$^{+/-}$*:HCVcpTg mice.* To further confirm the significance of persistent PPARα activation on core protein–induced pathological changes, *Ppara*$^{+/-}$ and *Ppara*$^{+/-}$:HCVcpTg mice were fed a standard diet containing 0.05% clofibrate for 24 months. Interestingly, hepatic steatosis appeared in the clofibrate-treated *Ppara*$^{+/-}$:HCVcpTg mice, but not in the *Ppara*$^{+/-}$ mice under the same treatment conditions (Figure 7, A and B). Similar to our observations in *Ppara*$^{+/+}$:HCVcpTg mice not treated with clofibrate, aberrant mitochondria with discontinuous outer membranes and decreased palmitic acid β-oxidation activity were found only in the clofibrate-treated *Ppara*$^{+/-}$:HCVcpTg mice (Figure 7, A and C). In addition, levels of MCAD mRNA; AOX, and CYP4A1 proteins; PPARα mRNA; and nuclear PPARα protein were higher in the clofibrate-treated *Ppara*$^{+/-}$:HCVcpTg mice than in the clofibrate-treated *Ppara*$^{+/-}$ mice (Figure 7, D–F), which suggests that the degree of PPARα activation in the former group was greater than that in the latter group and similar to that in *Ppara*$^{+/+}$:HCVcpTg mice not treated with clofibrate. Finally, the incidence of HCC after clofibrate treatment was higher in *Ppara*$^{+/-}$:HCVcpTg mice (25%; 5 in 20 mice) than in *Ppara*$^{+/-}$ mice (5%; 1 in 20 mice). Therefore, these results corroborate the importance of constant PPARα activation to the pathogenesis of hepatic steatosis and HCC in the transgenic mice.

Discussion

A novel and striking finding in this study is the absolute requirement of persistent PPARα activation for the development of HCV core protein–induced steatosis and HCC. Our data also show that the HCV core protein alone cannot induce steatosis and HCC in transgenic mice.

Mechanisms of development of steatosis in HCVcpTg mice were previously explained as an enhancement of de novo synthesis of fatty acids (29) and a decrease in MTP expression, the latter of which results in insufficient VLDL secretion from hepatocytes (30). In the present study, we revealed 2 novel mechanisms of steatogenesis in the transgenic mice, i.e., an impairment of mitochondrial β-oxidation due to the breakdown of mitochondrial outer membranes and an increase in fatty acid uptake into hepatocytes, associated with PPARα activation. PPARα activation, mitochondrial dysfunction, and hepatic steatosis appeared in 9-month-old *Ppara*$^{+/+}$:HCVcpTg mice and continued until 24 months of age, clearly preceding development of HCC. These findings thereby indicate a correlation between PPARα activation, hepatic steatosis, and HCC.

We obtained the novel and rather paradoxical finding that significant PPARα activation, which generally is expected to reduce hepatic triglyceride levels, is essential for the development of severe steatosis induced by HCV core protein. According to the results of this study, the following hypothesis concerning the development of steatosis in *Ppara*$^{+/+}$:HCVcpTg mice is proposed. First, the HCV core protein localizes partly in mitochondria (9). A recent study

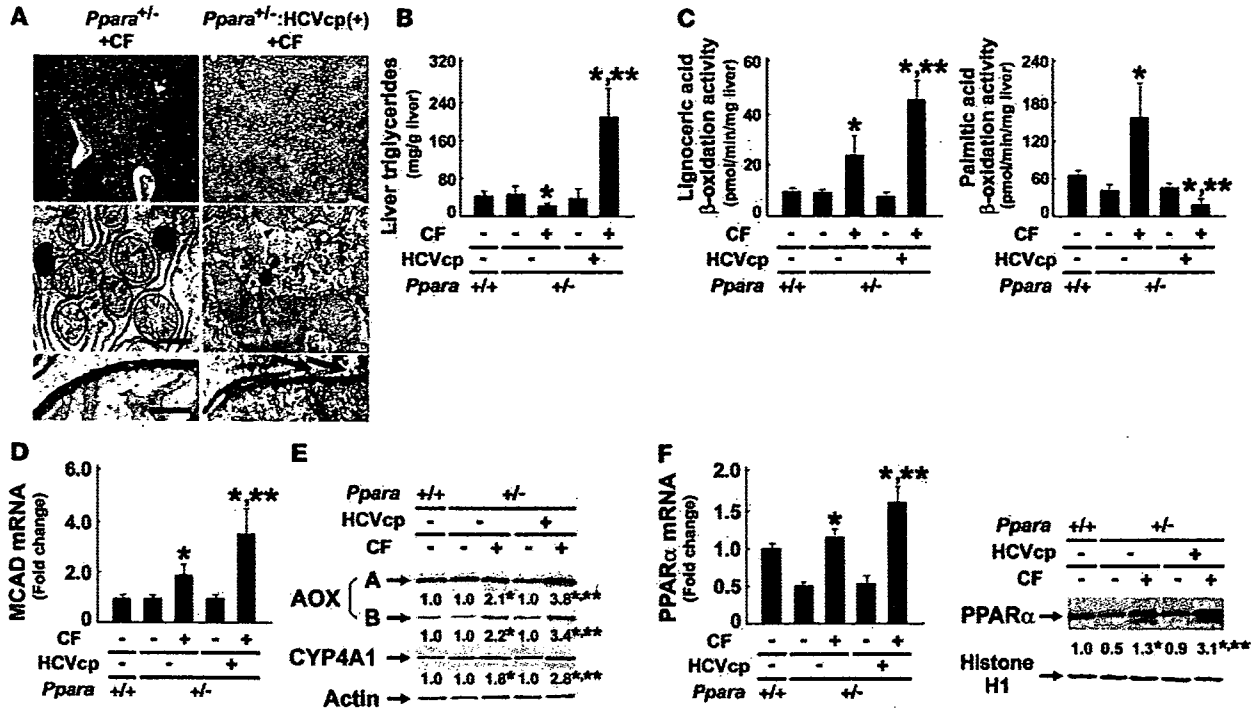

Figure 7

Development of hepatic steatosis by long-term treatment of clofibrate in *Ppara*$^{+/-}$:HCVcpTg mice. (**A**) Histological examination of *Ppara*$^{+/-}$ and *Ppara*$^{+/-}$:HCVcpTg mice treated with diet containing 0.05% (w/w) clofibrate for 24 months (CF). Top: Histological appearance of H&E-stained liver sections. Magnification, ×40. Microvesicular and macrovesicular steatosis were detected only in clofibrate-treated *Ppara*$^{+/-}$:HCVcpTg mice. Middle and bottom: Electron microscopic features of hepatic mitochondria. Some C-shaped mitochondria showing discontinuance of outer membranes (arrows) were found in clofibrate-treated *Ppara*$^{+/-}$:HCVcpTg mice. Scale bars: 400 nm (middle), 30 nm (bottom). (**B** and **C**) Content of liver triglycerides and lignoceric and palmitic acid β-oxidation activities. (**D**) MCAD mRNA levels. mRNA levels were normalized to those of GAPDH and subsequently normalized to those in *Ppara*$^{+/+}$ nontransgenic mice. (**E**) Immunoblot analysis of AOX and CYP4A1. Whole-liver lysate (20 μg protein) was loaded in each lane. Actin was used as a loading control. Results are representative of 6 independent experiments. (**F**) PPARα mRNA levels and nuclear PPARα contents. Left: PPARα mRNA levels. The same samples used in **D** were adopted. Right: Immunoblot analysis of nuclear PPARα. Nuclear fraction obtained from each mouse (100 μg protein) was loaded in each well. Histone H1 was used as a loading control. In **E** and **F**, the mean value of the fold changes is shown under each band. Results are representative of 6 independent experiments. Band intensity was quantified densitometrically, normalized to that of the loading control, and subsequently normalized to that in *Ppara*$^{+/+}$ nontransgenic mice. **P* < 0.05 compared with untreated mice of the same genotype; ***P* < 0.05 compared with clofibrate-treated *Ppara*$^{+/-}$ mice without core protein gene. Results are expressed as mean ± SD (*n* = 6/group).

showed that, in isolated mitochondria, the core protein directly increased Ca^{2+} influx, inhibited electron transport complex I activity, and induced ROS production (31), all of which can increase the fragility of mitochondria and depress mitochondrial function. In addition, the HCV core protein also localizes in nuclei (9) and can coexist in PPARα-RXRα heterodimer through a direct interaction with the DNA-binding domain of RXRα, which enhances the transcriptional activity of PPARα target genes, such as AOX, despite the absence of PPARα ligands in cultured cells (27). The HCV core protein can also be involved in the PPARα-RXRα complex through a direct interaction with cyclic-AMP responsive element binding protein-binding protein (32), which is able to bind to PPARα (33). Thus, the core protein probably serves as a coactivator and stabilizer of PPARα in vivo, which was further confirmed in this study. Moreover, because it is also known that the core protein itself activates ERK1/2 and p38 mitogen-activated protein kinase (34), these activations might phosphorylate PPARα and thereby transactivate it (35). The core protein–induced PPARα activation enhances the basal expression of AOX and CYP4A1, which leads to increased production of ROS and dicarboxylic acids. These toxic compounds can damage mitochondrial outer membranes, which impairs the mitochondrial β-oxidation system. These damages directly induce the accumulation of long-chain fatty acids in hepatocytes. Furthermore, PPARα activation increases the expression of FAT and FATP, which promotes the influx of fatty acids from blood. Long-chain fatty acids and their CoA esters accumulated in hepatocytes are likely to act as potent detergents, which further damages the outer membranes of mitochondria. Fatty acids and their derivatives function as natural ligands of PPARα, which results in the activation of PPARα and the induction of FAT, FATP, AOX, and CYP4A1, which further accelerates mitochondrial damage, the reduction of mitochondrial β-oxidation activity, and the accumulation of fatty acids in a vicious cycle.

Persistent PPARα activation increases oxidative DNA damage because of a disproportionate increase in ROS-generating enzymes relative to the levels of degrading enzymes such as catalase and SOD, which can predispose hepatocytes to malignant transformation. In addition, persistent PPARα activation leads to increased

Table 2
Primer pairs used for RT-PCR

Gene	GeneBank accession number		Primer sequence	Product (bp)
ACC	NM_133360	F	5′-GGGCACAGACCGTGGTAGTT-3′	105
		R	5′-CAGGATCAGCTGGGATACTGAGT-3′	
ApoB	NM_009693	F	5′-TCACCCCCGGGATCAAG-3′	85
		R	5′-TCCAAGGACACAGAGGGCTTT-3′	
AOX	NM_015729	F	5′-TGGTATGGTGTCGTACTTGAATGAC-3′	145
		R	5′-AATTTCTACCAATCTGGCTGCAC-3′	
FAS	NM_007988	F	5′-ATCCTGGAACGAGAACACGATCT-3′	140
		R	5′-AGAGACGTGTCACTCCTGGACTT-3′	
FAT	NM_007643	F	5′-CCAAATGAAGATGAGCATAGGACAT-3′	87
		R	5′-GTTGACCTGCAGTCGTTTTGC-3′	
FATP	NM_011977	F	5′-ACCACCGGGCTTCCTAAGG-3′	80
		R	5′-CTGTAGGAATGGTGGCCAAAG-3′	
GAPDH	M32599	F	5′-TGCACCACCAACTGCTTAG-3′	177
		R	5′-GGATGCAGGGATGATGTTCTG-3′	
L-FABP	NM_017399	F	5′-GCAGAGCCAGGAGAACTTTGAG-3′	121
		R	5′-TTTGATTTTCTTCCCTTCATGCA-3′	
MCAD	NM_007382	F	5′-TGCTTTTGATAGAACCAGACCTACAGT-3′	128
		R	5′-CTTGGTGCTCCACTAGCAGCTT-3′	
MTP	NM_008642	F	5′-GAGCGGTCTGGATTTACAACG-3′	72
		R	5′-GTAGGTAGTGACAGATGTGGCTTTTG-3′	
PPARα	NM_011144	F	5′-CCTCAGGGTACCACTACGGAGT-3′	69
		R	5′-GCCGAATAGTTCGCCGAA-3′	

F, forward sequence; R, reverse sequence.

cell division, as revealed by the expression of cell cycle regulators such as cyclin D1 and CDK4. Furthermore, there is little change in apoptosis, which, under normal circumstances, would remove damaged cells capable of undergoing transformation. Thus, under these conditions, it is plausible that some aberrant hepatocytes do not undergo apoptosis and develop into HCC.

It is well known that chronic activation of PPARα is associated with hepatocarcinogenesis in mice exposed to peroxisome proliferators or in mice lacking AOX expression. The common clinicopathological characteristics of HCC in these mice are multicentric HCC (20, 22, 36, 37), the well-differentiated appearance of HCC including trabecular features and often a "nodule-in-nodule" pattern (22, 36, 37), and no evidence of fibrosis or cirrhosis in the nonneoplastic liver parenchyma (22, 36), similar to that observed in *Ppara*$^{+/+}$:HCVcpTg mice. However, mice chronically exposed to peroxisome proliferators are clearly distinct from *Ppara*$^{+/+}$:HCVcpTg mice in that they have normal mitochondrial organization, increased mitochondrial β-oxidation activity, and no steatosis (16, 36). AOX-null mice are also different from *Ppara*$^{+/+}$:HCVcpTg mice with respect to mitochondrial structure (22). These detailed comparisons between the 3 mouse models reveal the importance of mitochondrial abnormalities in the pathogenesis of HCV-related diseases.

PPARα is known to regulate the hepatic expression of many proteins associated with fatty acid and triglyceride metabolism, cell division and apoptosis, oxidative stress generation and degradation, and so forth (15, 16, 20, 21, 24–26); therefore, complete deletion of the PPARα gene from mice might cause hitherto unknown influences on the pathways involved in the development of hepatic steatosis and HCC. To consider these unknown effects, *Ppara*$^{+/-}$:HCVcpTg mice were adopted in the current study. Surprisingly, almost all results from *Ppara*$^{+/-}$:HCVcpTg mice were similar to those from *Ppara*$^{-/-}$:HCVcpTg mice, which demonstrates that the presence of functional PPARα itself is not a prerequisite for the occurrence of steatosis and HCC induced by the HCV core protein. Moreover, a comparison between *Ppara*$^{+/-}$:HCVcpTg and *Ppara*$^{+/+}$:HCVcpTg mice uncovered an unexpected and important fact that the core protein–dependent pathological changes do not appear without significant activation of PPARα. Thus, it is not the presence of PPARα per se, but rather a high level of PPARα activation that seems to be essential for the development of HCV core protein–induced steatosis and HCC.

To reinforce the abovementioned hypothesis, *Ppara*$^{+/-}$ and *Ppara*$^{+/-}$:HCVcpTg mice were treated with an exogenous PPAR agonist, clofibrate, for 24 months. In *Ppara*$^{+/-}$ mice, long-term clofibrate treatment caused a certain level of persistent PPARα activation and a low incidence of HCC. Interestingly, in *Ppara*$^{+/-}$:HCVcpTg mice, clofibrate treatment induced more intensive PPARα activation and HCC at a much higher incidence, accompanied by damaged mitochondrial outer membranes, severe steatosis, and decreased mitochondrial β-oxidation activity. The results from the clofibrate-treated *Ppara*$^{+/-}$:HCVcpTg mice were similar to those of the *Ppara*$^{+/+}$:HCVcpTg mice not treated with clofibrate. Therefore, these findings further support the concept that a long-term and high level of PPARα activation is necessary for steatogenesis and hepatocarcinogenesis in HCVcpTg mice and emphasize the significant role of the HCV core protein as a PPARα coactivator in vivo.

A pulse-chase experiment showed that PPARα was stabilized in hepatocyte nuclei in mice expressing the HCV core protein. Many nuclear receptors, including PPARα and RXRα, are known to be degraded by the ubiquitin-proteasome system (38), which plays an important role in modulating the activity of nuclear receptors. Further studies will be needed to clarify whether the core protein influences the ubiquitin-proteasome pathway.

Recent studies have shown conflicting result, i.e., that PPARα was downregulated in the livers of chronic hepatitis C patients (39, 40). Although the association between PPARα function and chronic HCV infection remains a matter of controversy in humans, the changes observed in the transgenic mice resemble in many ways the clinicopathological features of chronically HCV-infected patients; both show a high frequency of accompanying steatosis (10, 40, 41), increased accumulation of carbon 18 monounsaturated fatty acids in the liver (42), mitochondrial dysfunction (43), increased insulin resistance (44) and oxidative stress (45, 46), male-preferential (2) and multicentric occurrence of HCC (47, 48), and the well-differentiated appearance of HCC, including trabecular features and often a "nodule-in-nodule" pattern (47, 48). Thus, it is postulated that the mechanism of steatogenesis and hepatocarcinogenesis we proposed may partially apply to patients with chronic HCV infection. If so, therapeutic interventions to alleviate persistent and excessive PPARα activation might be beneficial in the prevention of HCC. To clarify the exact relationship between PPARα activation and HCV-induced hepatocarcinogenesis in humans, further

experiments using noncancerous liver tissues obtained from HCV-related HCC patients and using mice carrying human PPARα and HCV core protein genes are needed.

In conclusion, we clarified for the first time that persistent and potent PPARα activation is absolutely required for the development of severe steatosis and HCC induced by HCV core protein. In addition, we uncovered paradoxical and specific functions of PPARα in the mechanism of steatogenesis mediated by the core protein. Our results offer clues in the search for novel therapeutic and nutritional management options, especially with respect to neutral lipids, for chronically HCV-infected patients.

Methods

Mice. The generation of HCVcpTg mice and *Ppara*$^{-/-}$ mice was described previously (7, 24, 49). Male HCVcpTg mice and female *Ppara*$^{-/-}$ mice were mated, and F1 mice bearing the HCV core protein gene were intercrossed to produce F2 mice. *Ppara*$^{+/+}$, *Ppara*$^{+/-}$, and *Ppara*$^{-/-}$ mice bearing the HCV core protein gene, designated as *Ppara*$^{+/+}$:HCVcpTg, *Ppara*$^{+/-}$:HCVcpTg, and *Ppara*$^{-/-}$:HCVcpTg mice, in the F4 generation were subjected to serial analyses. Because HCC develops preferentially in male HCVcpTg mice (9), male mice were analyzed. Age-matched male *Ppara*$^{+/+}$ mice without the core protein gene were used as controls. For identifying genotypes, genomic DNA was isolated from mouse tails and amplified by PCR. Primer pairs were designed as described elsewhere: 5′-GCCCACAGGACGTTAAGTTC-3′ and 5′-TAGTTCACGCCGTCCTCCAG-3′ for the HCV core gene (7) and 5′-CAGAGCAACCATCCAGATGA-3′ and 5′-AAACGCAACGTAGAGTGCTG-3′ for the PPARα gene (24). Amplified alleles for HCV core and PPARα genes were 460 and 472 base pairs, respectively. Five mice per cage were fed a routine diet and were kept free of specific pathogens according to institutional guidelines. For the clofibrate treatment experiments, 2-month-old male *Ppara*$^{+/-}$ and *Ppara*$^{+/-}$:HCVcpTg mice were randomly divided into 2 groups (n = 20 in each group) and were fed either a routine diet or one containing 0.05% (w/w) clofibrate (Wako Pure Chemicals Industries) for 24 months. All mice were killed by cervical dislocation before their livers were excised. If a hepatic tumor was present, the tumor was removed and subjected to histological analysis, and the remaining liver tissues were used for biochemical analyses. All animal experiments were conducted in accordance with animal study protocols outlined in the *Guide for the Care and Use of Laboratory Animals* prepared by the National Academy of Sciences and approved by the Shinshu University School of Medicine.

Preparation of nuclear, mitochondrial, and cytosolic fractions. Approximately 400 mg of liver tissue was minced on ice and transferred to 10% (w/v) isolation buffer (250 mM sucrose in 10 mM Tris-HCl [pH 7.4] and 0.5 mM EGTA and 0.1% bovine serum albumin [pH 7.4]). The samples were gently homogenized by 10–20 strokes with a chilled Dounce homogenizer (Wheaton) and loose-fitting pestle. The homogenate was centrifuged at 500 × *g* for 5 min at 4°C. The supernatant was retained, and the resulting pellet was resuspended with isolation buffer and centrifuged at 4,500 *g* for 10 min at 4°C. The pellet fraction was suspended again and centrifuged at 20,000 × *g* for 1 h at 4°C, and the resulting pellet was used as the nuclear fraction. The combined supernatant fractions were centrifuged at 7,800 × *g* for 10 min at 4°C to obtain a crude mitochondria pellet. This pellet was resuspended with isolation buffer, centrifuged at 7,800 × *g* for 10 min at 4°C, and used as the mitochondrial fraction. Finally, all supernatant fractions were collected and centrifuged at 20,000 × *g* for 30 min at 4°C, and the resulting supernatant was used as the cytosolic fraction.

Immunoblot analysis. Protein concentrations were measured colorimetrically with a BCA Protein Assay kit (Pierce). For the analysis of fatty acid-metabolizing enzymes, hepatocyte mitochondrial fractions or whole-liver lysates (20 μg protein) were subjected to 10% SDS-PAGE (16). For analysis of PPARα, nuclear fractions (100 μg protein) were used. For analysis of other proteins, whole lysates or cytosolic fractions (50 μg protein) were subjected to electrophoresis. After electrophoresis, the proteins were transferred to nitrocellulose membranes, which were incubated with the primary antibody and then with alkaline phosphatase-conjugated goat anti-rabbit or anti-mouse IgG. Antibodies against HCV core protein, fatty acid–metabolizing enzymes, CYP4A1, catalase, and PPARα were described previously (9, 16, 24, 50). Antibodies against other proteins were purchased commercially: cytochrome *c* antibody from BD Transduction Laboratories and other antibodies from Santa Cruz Biotechnology. The band of actin or histone H1 was used as the loading control. The band intensity was measured densitometrically, normalized to that of actin or histone H1, and subsequently expressed as fold changes relative to that of *Ppara*$^{+/+}$ nontransgenic mice.

Analysis of mRNA. Total liver RNA was extracted using an RNeasy Mini Kit (Qiagen), and cDNA was generated by SuperScript II reverse transcriptase (Gibco BRL). Quantitative RT-PCR was performed using a SYBR green PCR kit and an ABI Prism 7700 Sequence Detection System (Applied Biosystems). The primer pairs used for RT-PCR are shown in Table 2. The mRNA level was normalized to the GAPDH mRNA level and subsequently expressed as fold changes relative to that of *Ppara*$^{+/+}$ nontransgenic mice.

Light microscopy and immunohistochemical analysis. Small blocks of liver tissue from each mouse were fixed in 10% formalin in phosphate-buffered saline and embedded in paraffin. Sections (4 μm thick) were stained with hematoxylin and eosin. For immunohistochemical localization of PCNA and 8-OHdG, other small blocks of liver tissue were fixed in 4% paraformaldehyde in phosphate-buffered saline. Sections (4 μm thick) then were affixed to glass slides and incubated overnight with mouse monoclonal antibodies against PCNA (1:100 dilution; Santa Cruz) or 8-OHdG (1:10 dilution; Japan Institute for the Control of Aging). Sections were immunostained using EnVision+ kit, with 3,3′-diaminobenzidine as a substrate (DAKO). Hepatocytes positive for PCNA or 8-OHdG were examined in 10 randomly selected ×400 microscopic fields per section. Two-thousand hepatocytes were examined for each mouse, and the number of immunostained hepatocyte nuclei was expressed as a percentage.

Assessment of hepatocyte apoptosis. TUNEL assay was performed using a MEBSTAIN Apoptosis Kit II (Medical & Biological Laboratories). Two thousand hepatocytes were examined for each mouse, and the number of TUNEL-positive hepatocytes was expressed as a percentage.

Pulse-label and pulse-chase experiments. Parenchymal hepatocytes were isolated by the modified *in situ* perfusion method (51). After perfusion with 0.05% collagenase solution (Wako), the isolated hepatocytes were washed 3 times by means of differential centrifugation and the dead cells were removed by density-gradient centrifugation at 500 *g* for 3 min at 4°C on Percoll (Amersham Pharmacia Biotech). The live hepatocytes were washed and suspended in William's E medium containing 5% FBS. When the viability of the isolated hepatocytes exceeded 85% as determined by the trypan blue exclusion test, the following experiments were conducted. The isolated hepatocytes were washed twice and incubated in methionine-free medium containing 5% dialyzed FBS for 1 h at 37°C. The medium was replaced with the same medium containing 300 mCi/ml of [^{35}S]methionine (Amersham Pharmacia Biotech). After a 3-h incubation, the labeled medium was exchanged for the standard medium, and the preparation was chased for 3, 6, or 12 h. The labeled cells were washed, homogenized, and centrifuged at 800 *g* for 5 min at 4°C to obtain a crude nucleus pellet. This pellet was resuspended with isolation buffer and centrifuged at 20,000 *g* for 1 h at 4°C to prepare the nuclear fraction. The levels of radioactivity in the homogenates of the pulse-labeled preparations were similar between the transgenic and the nontransgenic mice, which suggested that the [^{35}S]methionine uptake capacity in the former hepatocytes was similar to that in the latter. The nuclear fraction was lysed in RIPA buffer (10 mM Tris-HCl, pH 7.4; 0.2% sodium deoxycholate, 0.2% Nonidet P-40, 0.1% SDS,

0.25 mM PMSF, and 10 mg/ml aprotinin). The lysate was incubated for 3 h at 4°C with purified anti-PPARα antibody. The immune complexes were precipitated with *Staphylococcus aureus* protein A bound to agarose beads. After the precipitates had been washed in RIPA buffer, the labeled proteins were resolved by 10% SDS-PAGE and visualized by autoradiography.

Analysis of fatty acid uptake ability. Assays for fatty acid uptake were carried out according to a method reported by Graulet et al. (52) with minor modifications. Briefly, 3 mice in each group were fasted overnight. Livers were removed quickly, rinsed in ice-cold saline solution, and cut into 500-μm thick slices with an Oxford Vibratome (Oxford Laboratories). Approximately 150 mg of fresh liver (6–8 liver slices) was placed on stainless steel grids positioned in a 25-ml flask equipped with suspended plastic center wells (Kontes) and incubated in RPMI-1640 medium (Sigma-Aldrich) devoid of fatty acids for 2 h at 37°C. The medium was then replaced with fresh RPMI-1640 medium supplemented with an antibiotic-antimycotic cocktail and 0.8 mM [1-^{14}C]palmitic acid (4 mCi/mmol) (American Radiolabeled Chemicals) complexed to BSA (palmitic acid:albumin molar ratio of 4:1). After a 7-h incubation, the medium was collected and slices were washed with 2 ml of saline solution and homogenized in Tris buffer (25 mM Tris-HCl, pH 8.0; 50 mM NaCl). Fatty acid uptake ability was calculated as the sum of palmitic acid converted to CO_2 and ketone bodies with that incorporated into total cellular lipids after incubation. For measurement of CO_2 production by the liver slices, the center wells were placed into scintillation vials containing 4 ml of scintillation cocktail, and radioactivity was counted. For measurement of ketone body generation, aliquots of medium (500 μl) and liver homogenates (250 μl) were treated with ice-cold perchloric acid to make final concentrations of 200 mM and were centrifuged at 3,000 *g* for 20 min at 4°C. Aliquots of the supernatant containing the ketone bodies were introduced into the scintillation vials, and radioactivity was counted. Total cellular lipids were extracted from the liver homogenates according to a modified method developed by Folch et al. (53), collected into scintillation vials, and evaporated to dryness under an air stream; radioactivity was then counted. The experiment was repeated 3 times, and palmitic acid uptake ability was expressed as fold changes relative to that of *Ppara*$^{+/+}$ nontransgenic mice.

Other methods. To determine the hepatic content of lipids and lipid peroxides, lipids were extracted according to a method by Folch et al. (53). Triglycerides and free fatty acids were measured with a Triglyceride E-test kit and a NEFA C-test kit (Wako), respectively. Lipid peroxides (malondialdeyde and 4-hydroxyalkenals) were measured using an LPO-586 kit (OXIS International). Hepatic β-oxidation activity was determined as described previously (16). Hepatic caspase 3 activity was measured as described elsewhere (54). Plasma glucose and insulin levels were determined using a Glucose CII-test kit (Wako) and a mouse insulin ELISA kit (U-type, AKRIN-031; Shibayagi), respectively.

Statistics. Statistical analysis was performed with a 2-tailed Student's *t* test for quantitative variables or with a chi-square test for qualitative variables. Quantitative data are expressed as the mean ± SD. $P < 0.05$ was considered to be statistically significant.

Acknowledgments

We thank Trevor Ralph for editorial assistance and Chikako Tanaka for helpful suggestions.

Received for publication August 13, 2007, and accepted in revised form November 7, 2007.

Address correspondence to: Naoki Tanaka, Department of Metabolic Regulation, Institute on Aging and Adaptation, Shinshu University Graduate School of Medicine, Asahi 3-1-1, Matsumoto 390-8621, Japan. Phone: 81-263-37-2850; Fax: 81-263-37-3094; E-mail: naopi@hsp.md.shinshu-u.ac.jp.

1. Kiyosawa, K., et al. 1990. Interrelationship of blood transfusion, non-A, non-B hepatitis and hepatocellular carcinoma: analysis by detection of antibody to hepatitis C virus. *Hepatology.* **12**:671–675.
2. Kiyosawa, K., et al. 2004. Hepatocellular carcinoma: recent trends in Japan. *Gastroenterology.* **127**(5 Suppl. 1):S17–S26.
3. Tanaka, Y., et al. 2002. Inaugural article: a comparison of the molecular clock of hepatitis C virus in the United States and Japan predicts that hepatocellular carcinoma incidence in the United States will increase over the next two decades. *Proc. Natl. Acad. Sci. U. S. A.* **99**:15584–15589.
4. Okuda, K., Fujimoto, I., Hanai, A., and Urano, Y. 1987. Changing incidence of hepatocellular carcinoma in Japan. *Cancer Res.* **47**:4967–4972.
5. El-Serag, H.B., and Mason, A.C. 1999. Rising incidence of hepatocellular carcinoma in the United States. *N. Engl. J. Med.* **340**:745–750.
6. Shimotohno, K. 2000. Hepatitis C virus and its pathogenesis. *Semin. Cancer Biol.* **10**:233–240.
7. Moriya, K., et al. 1997. Hepatitis C virus core protein induces hepatic steatosis in transgenic mice. *J. Gen. Virol.* **78**:1527–1531.
8. Shintani, Y., et al. 2004. Hepatitis C virus infection and diabetes: direct involvement of the virus in the development of insulin resistance. *Gastroenterology.* **126**:840–848.
9. Moriya, K., et al. 1998. The core protein of hepatitis C virus induces hepatocellular carcinoma in transgenic mice. *Nat. Med.* **4**:1065–1068.
10. Powell, E.E., Jonsson, J.R., and Clouston, A.D. 2005. Steatosis: co-factor in other liver diseases. *Hepatology.* **42**:5–13.
11. Ohata, K., et al. 2003. Hepatic steatosis is a risk factor for hepatocellular carcinoma in patients with chronic hepatitis C virus infection. *Cancer.* **97**:3036–3043.
12. Browning, J.D., and Horton, J.D. 2004. Molecular mediators of hepatic steatosis and liver injury. *J. Clin. Invest.* **114**:147–152.
13. Le, T.H., et al. 2004. The zonal distribution of megamitochondria with crystalline inclusions in nonalcoholic steatohepatitis. *Hepatology.* **39**:1423–1429.
14. Yang, S., Lin, H.Z., Hwang, J., Chacko, V.P., and Diehl, A.M. 2001. Hepatic hyperplasia in noncirrhotic fatty livers: is obesity-related hepatic steatosis a premalignant condition? *Cancer Res.* **61**:5016–5023.
15. Desvergne, B., and Wahli, W. 1999. Peroxisome proliferator-activated receptors: nuclear control of metabolism. *Endocr. Rev.* **20**:649–688.
16. Aoyama, T., et al. 1998. Altered constitutive expression of fatty acid-metabolizing enzymes in mice lacking the peroxisome proliferator-activated receptor α (PPARα). *J. Biol. Chem.* **273**:5678–5684.
17. Staels, B., et al. 1998. Mechanism of action of fibrates on lipid and lipoprotein metabolism. *Circulation.* **98**:2088–2093.
18. Harano, Y., et al. 2006. Fenofibrate, a peroxisome proliferator-activated receptor α agonist, reduces hepatic steatosis and lipid peroxidation in fatty liver Shionogi mice with hereditary fatty liver. *Liver Int.* **26**:613–620.
19. Yeldandi, A.V., Rao, M.S., and Reddy, J.K. 2000. Hydrogen peroxide generation in peroxisome proliferator-induced oncogenesis. *Mutat. Res.* **448**:159–177.
20. Yu, S., Rao, M.S., and Reddy, J.K. 2003. Peroxisome proliferator-activated receptors, fatty acid oxidation, steatohepatitis and hepatocarcinogenesis. *Curr. Mol. Med.* **3**:561–572.
21. Peters, J.M., Cattley, R.C., and Gonzalez, F.J. 1997. Role of PPARα in the mechanism of action of the nongenotoxic carcinogen and peroxisome proliferator Wy-14,643. *Carcinogenesis.* **18**:2029–2033.
22. Fan, C.Y., et al. 1998. Steatohepatitis, spontaneous peroxisome proliferation and liver tumors in mice lacking peroxisomal fatty acyl-CoA oxidase. Implications for peroxisome proliferator-activated receptor α natural ligand metabolism. *J. Biol. Chem.* **273**:15639–15645.
23. Moriya, K., et al. 2001. Oxidative stress in the absence of inflammation in a mouse model for hepatitis C virus-associated hepatocarcinogenesis. *Cancer Res.* **61**:4365–4370.
24. Lee, S.S., et al. 1995. Targeted disruption of the α isoform of the peroxisome proliferator-activated receptor gene in mice results in abolishment of the pleiotropic effects of peroxisome proliferators. *Mol. Cell. Biol.* **15**:3012–3022.
25. Mandard, S., Muller, M., and Kersten, S. 2004. Peroxisome proliferator-activated receptor α target genes. *Cell. Mol. Life Sci.* **61**:393–416.
26. Peters, J.M., et al. 1998. Role of peroxisome proliferator-activated receptor α in altered cell cycle regulation in mouse liver. *Carcinogenesis.* **19**:1989–1994.
27. Tsutsumi, T., et al. 2002. Interaction of hepatitis C virus core protein with retinoid X receptor α modulates its transcriptional activity. *Hepatology.* **35**:937–946.
28. Tanaka, N., et al. 2003. In vivo stabilization of nuclear retinoid X receptor α in the presence of peroxisome proliferator-activated receptor α. *FEBS Lett.* **543**:120–124.
29. Moriishi, K., et al. 2007. Critical role of PA28γ in hepatitis C virus-associated steatogenesis and hepatocarcinogenesis. *Proc. Natl. Acad. Sci. U. S. A.* **104**:1661–1666.
30. Perlemuter, G., et al. 2002. Hepatitis C virus core

protein inhibits microsomal triglyceride transfer protein activity and very low density lipoprotein secretion: a model of viral-related steatosis. *FASEB J.* **16**:185–194.
31. Korenaga, M., et al. 2005. Hepatitis C virus core protein inhibits mitochondrial electron transport and increases reactive oxygen species (ROS) production. *J. Biol. Chem.* **280**:37481–37488.
32. Gomez-Gonzalo, M., et al. 2004. Hepatitis C virus core protein regulates p300/CBP co-activation function. Possible role in the regulation of NF-AT1 transcriptional activity. *Virology.* **328**:120–130.
33. Yu, S., and Reddy, J.K. 2007. Transcription coactivators for peroxisome proliferator-activated receptors. *Biochim. Biophys. Acta.* **1771**:936–951.
34. Spaziani, A., Alisi, A., Sanna, D., and Balsano, C. 2006. Role of p38 MAPK and RNA-dependent protein kinase (PKR) in hepatitis C virus core-dependent nuclear delocalization of cyclin B1. *J. Biol. Chem.* **281**:10983–10989.
35. Diradourian, C., Girard, J., and Pegorier, J.P. 2005. Phosphorylation of PPARs: from molecular characterization to physiological relevance. *Biochimie.* **87**:33–38.
36. Reddy, J.K., Rao, M.S., Azarnoff, D.L., and Sell, S. 1979. Mitogenic and carcinogenic effects of a hypolipidemic peroxisome proliferator, [4-chloro-6-(2,3-xylidino)-2- pyrimidinylthio]acetic acid (Wy-14,643), in rat and mouse liver. *Cancer Res.* **39**:152–161.
37. Rao, M.S., and Reddy, J.K. 1996. Hepatocarcinogenesis of peroxisome proliferators. *Ann. N. Y. Acad. Sci.* **804**:573–587.
38. Genini, D., and Catapano, C.V. 2006. Control of peroxisome proliferator-activated receptor fate by the ubiquitin-proteasome system. *J. Recept. Signal. Transduct. Res.* **26**:679–692.
39. Dharancy, S., et al. 2005. Impaired expression of the peroxisome proliferator-activated receptor alpha during hepatitis C virus infection. *Gastroenterology.* **128**:334–342.
40. de Gottardi, A., et al. 2006. Peroxisome proliferator-activated receptor-alpha and -gamma mRNA levels are reduced in chronic hepatitis C with steatosis and genotype 3 infection. *Aliment. Pharmacol. Ther.* **23**:107–114.
41. Lefkowitch, J.H., et al. 1993. Pathological diagnosis of chronic hepatitis C: a multicenter comparative study with chronic hepatitis B. *Gastroenterology.* **104**:595–603.
42. Moriya, K., et al. 2001. Increase in the concentration of carbon 18 monounsaturated fatty acids in the liver with hepatitis C: analysis in transgenic mice and humans. *Biochem. Biophys. Res. Commun.* **281**:1207–1212.
43. Barbaro, G., et al. 1999. Hepatocellular mitochondrial alterations in patients with chronic hepatitis C: ultrastructural and biochemical findings. *Am. J. Gastroenterol.* **94**:2198–2205.
44. Hui, J.M., et al. 2003. Insulin resistance is associated with chronic hepatitis C virus infection and fibrosis progression [corrected]. *Gastroenterology.* **125**:1695–1704.
45. Kato, J., et al. 2001. Normalization of elevated hepatic 8-hydroxy-2'-deoxyguanosine levels in chronic hepatitis C patients by phlebotomy and low iron diet. *Cancer Res.* **61**:8697–8702.
46. Horiike, S., et al. 2005. Accumulation of 8-nitroguanine in the liver of patients with chronic hepatitis C. *J. Hepatol.* **43**:403–410.
47. Takenaka, K., et al. 1994. Possible multicentric occurrence of hepatocellular carcinoma: a clinicopathological study. *Hepatology.* **19**:889–894.
48. Oikawa, T., et al. 2005. Multistep and multicentric development of hepatocellular carcinoma: histological analysis of 980 resected nodules. *J. Hepatol.* **42**:225–229.
49. Akiyama, T.E., et al. 2001. Peroxisome proliferator-activated receptor-α regulates lipid homeostasis, but is not associated with obesity. *J. Biol. Chem.* **276**:39088–39093.
50. Nakajima, T., et al. 2004. Peroxisome proliferator-activated receptor α protects against alcohol-induced liver damage. *Hepatology.* **40**:972–980.
51. Ni, R., et al. 1994. Fas-mediated apoptosis in primary cultured mouse hepatocytes. *Exp. Cell Res.* **215**:332–337.
52. Graulet, B., Gruffat, D., Durand, D., and Bauchart, D. 1998. Fatty acid metabolism and very low density lipoprotein secretion in liver slices from rats and preruminant calves. *J. Biochem.* **124**:1212–1219.
53. Folch, J., Lees, M., and Sloane Stanley, G.H. 1957. A simple method for the isolation and purification of total lipids from animal tissues. *J. Biol. Chem.* **226**:497–509.
54. Gurtu, V., Kain, S.R., and Zhang, G. 1997. Fluorometric and colorimetric detection of caspase activity associated with apoptosis. *Anal. Biochem.* **251**:98–102.

J Gastroenterol 2007; 42:329–335
DOI 10.1007/s00535-007-2034-z

Journal of Gastroenterology

Review

Drug resistance in antiviral treatment for infections with hepatitis B and C viruses

HIROSHI YOTSUYANAGI and KAZUHIKO KOIKE

Department of Infectious Diseases, Internal Medicine, Graduate School of Medicine, University of Tokyo, 7-3-1 Hongo, Bunkyo-ku, Tokyo 113-8655, Japan

Treatments for infections with hepatitis B and C viruses have recently developed markedly, and range from nonspecific interferon-based treatments to specific antiviral treatments, such as those that inhibit hepatitis virus-coded protein production or activity. These developments have contributed to the achievement of excellent enhancement of the antiviral effect. On the other hand, the development of specific antiviral therapies has created unprecedented problems. Antiviral drug-resistant strains of viruses have emerged, leading to a poor prognosis for infected patients. Clarification of the mechanisms underlying the emergence of such resistance to drugs will be useful for the treatment of such patients. In this review, we outline pathological conditions associated with hepatitis B and C viruses and their treatments, and discuss the current situation and mechanisms underlying the emergence of antiviral drug-resistant strains.

Key words: Interferon, lamivudine, entecavir, adefovir, ribavirin

Introduction

Infections with hepatitis B and C viruses (HBV and HCV, respectively) are a problem worldwide. Many patients are infected with HBV and HCV, and these infections are not only a major medical burden but also a socioeconomic burden because of their possible progression from chronic hepatitis to cirrhosis and hepatocellular carcinoma (HCC) if left untreated.[1,2] The treatments against these hepatitis viruses have been mainly nonspecific, based on the use of interferon (IFN). Specific antiviral drugs developed recently that inhibit hepatitis viral replication, for example, by inhibition of reverse transcriptase in HBV, have shown remarkable efficacy.[3,4] However, these treatments have also turned out to be a double-edged sword because they have led to the emergence of strains resistant to these drugs. The emergence of antiviral drug-resistant strains of these viruses may hinder the development of treatments against them.

Received: February 21, 2007 / Accepted: February 25, 2007
Reprint requests to: H. Yotsuyanagi

HBV infection

HBV belongs to the family *Hepadnaviridae*. HBV is a DNA virus that has an approximately 3.2-kb circular incomplete double-stranded DNA genome. When it replicates, HBV forms DNA by using its own reverse transcriptase with RNA as a replicative intermediate. Worldwide, the distribution of HBV carriers and the incidence of HCC are closely correlated. The number of HBV carriers in Japan is estimated to be approximately one million, many of whom became infected via perinatal mother-to-child transmission. Hepatitis B e antigen (HBeAg) is a protein produced by the wild-type HBV strain as it replicates that appears in the blood. Generally, the presence of HBeAg indicates an abundance of the virus, and the detection of anti-HBe antibody often indicates a marked decrease in the HBV load.

HBV carriers are HBeAg-positive asymptomatic carriers (AsC) in the early stages of HBV infection. Their blood HBV level is very high in these stages. They can develop symptoms of hepatitis at any time of their life, but generally do between adolescence and their early 30s. At that time, the HBV load decreases markedly, and symptoms of hepatitis improve in 2 to 3 years in 80%–90% of HBV patients. Most of these patients then become negative for HBeAg and positive for the anti-HBe antibody. The annual incidence of seroconversion from being HBeAg-positive to anti-HBe antibody-

positive has been reported to be approximately 5%.[5,6] However, symptoms of hepatitis persist in about 10%–20% of these patients even after seroconversion; such patients often develop cirrhosis and HCC.[7]

Treatment of HBV infection

There are several choices for treatment of chronic hepatitis B, but they all have limited efficacy. HBV elimination [i.e., serum HB surface antigen (HBsAg)-negative status] is difficult in HBV carriers. Seroconversion from HBeAg-positive to anti-HBe antibody-positive is generally the goal of HBV infection treatment. It should also be understood that many HBV AsCs do not need to or often must not undergo treatment with any anti-HBV agent.

In approximately 80% of patients with chronic hepatitis B, seroconversion occurs spontaneously. Consequently, chronic hepatitis B does not progress to cirrhosis in most chronic hepatitis B patients. The 15%–20% of HBV carriers who do not show seroconversion ultimately develop cirrhosis and/or HCC and should undergo antiviral treatment for chronic hepatitis B. IFN and reverse transcriptase inhibitors, including lamivudine, adefovir dipivoxil, and entecavir, have been approved for the treatment of chronic hepatitis B. Among these, lamivudine was the first used for chronic hepatitis B patients.

Lamivudine recipients are more likely than placebo recipients to show a histological response (52% vs. 23%, $P < 0.001$), the disappearance of HBeAg in serum (32% vs. 11%, $P = 0.003$), a sustained decrease in serum HBV DNA level to undetectable levels (44% vs. 16%, $P < 0.001$), and a sustained normalization of the serum alanine aminotransferase (ALT) level (41% vs. 7 %, $P < 0.001$) after 52 weeks of treatment.[8]

Entecavir has an antiviral effect comparable to that of lamivudine. In one study of HBeAg-positive patients,[9] histological improvement after 48 weeks occurred in 226 of 314 patients in an entecavir-treated group (72%) and in 195 of 314 patients in a lamivudine-treated group (62%, $P = 0.009$). More patients in the entecavir-treated group than in the lamivudine-treated group had undetectable serum HBV DNA levels according to a polymerase chain reaction (PCR) assay (67% vs. 36%, $P < 0.001$), and normalization of ALT levels (68% vs. 60%, $P = 0.02$). However, the seroconversion rate was not very high in either group.

Emergence of antiviral resistance in HBV infection

The treatment efficacy against HBV infection has improved, as mentioned above. The primary reason for chronic hepatitis B becoming resistant to treatment is the emergence of drug-resistant strains.

Mechanisms underlying development of resistance to IFN-based treatments

IFNs are administered in a wide range of doses according to various protocols for chronic hepatitis B. Such variation in protocols must be taken into account in determining the therapeutic efficacy of such drugs. Viral factors potentially involved in drug resistance include the HBV genotype and the presence of HBeAg, a precore gene mutation, or a core promoter mutation. HBeAg negativity, HBV genotypes C and D, precore gene 1896 mutation, and 1762/1764 mutations in the core promoter have been reported to be responsible for a poor response to IFN treatment. Strictly, these factors do not indicate "drug resistance" to IFN. The acquisition of the precore gene 1896 mutation also decreases the efficacy of IFN treatment.[10]

Mutation of the HBV polymerase domain

The HBV polymerase (*Pol*) gene is shown in Fig. 1. The Pol/RT region of this gene encodes HBV reverse transcriptase (RT). In HBV gene replication, reverse transcription from pregenomic RNA to viral gene DNA occurs, and reverse transcriptase is used in this process. The Pol/RT region is further divided into five domains from A to E. The Pol/RT active center is reported to be in domain C, domains B and E have been reported to be important for RNA template binding, and domains A and D for binding to nucleic acids.

Nucleic acid analog formulations are incorporated into the viral genome involved in reverse transcription instead of nucleic acids to inhibit viral replication competitively. However, if a Pol/RT gene mutation emerges, the nucleic acid analog formulation administered may be unable to inhibit viral replication because of interference with its binding to RT. Acquisition of this mutation of the Pol/RT gene thus results in the emergence of a drug-resistant viral strain. This mutation is shown in Fig. 1.

Resistance to lamivudine

Among nucleic acid analog formulations, lamivudine (LAM) has been used longest for the treatment of chronic hepatitis B , and its use continued until resistance to this drug emerged. Many factors underlying this resistance have been identified.

LAM resistance is caused by a mutation in which the 204th methionine (M) in the polymerase domain is replaced by valine (V) or isoleucine (I) (rtM204V/I). Because the site containing the 204th methionine is referred to as the YMDD motif, this mutation is also called the YVDD mutation or YIDD mutation. Another mutation associated with rtM204V/I is caused by replacement of the 180th leucine (L) by M (rtL180M).

rtM204V/I was detected in 10% of HBeAg-positive patients with chronic hepatitis B 24 weeks after the start